

~~Subglacial upwelling in winter/~~**Early spring** ~~increases~~**submarine discharge plumes** **fuel** under-ice primary production

Tobias Reiner Vonnahme¹, Emma Persson¹, Ulrike Dietrich¹, Eva Hejdukova², Christine Dybwad¹, Josef Elster³, Melissa Chierici^{4,5}, Rolf Gradinger¹

¹ Department of Arctic and Marine Biology, UiT – The Arctic University of Norway, Tromsø, Norway

² Department of Ecology, Faculty of Science, Charles University, Prague, Czech Republic

³ University of South Bohemia, České Budějovice, and Institute of Botany ASCR, Třeboň, Czech Republic

⁴ Institute of Marine Research, Tromsø, Norway

⁵ University Centre in Svalbard (UNIS), Longyearbyen, Svalbard, Norway

Correspondence to: Tobias R. Vonnahme (~~Tobias.Vonnahme@uit.no~~ T.r.vonnahme@gmail.com)

Abstract. Subglacial upwelling of nutrient rich bottom water ~~is known to can support high~~sustain elevated summer primary production in ~~Aretie~~tidewater glacier influenced fjord systems. However, ~~during the winter/spring~~early spring season, the importance of subglacial upwelling has not been considered yet during the early spring season. We hypothesized that ~~subglacial submarine upwelling-discharge~~ under sea ice is present in ~~winter/spring~~early spring and sufficient to increase phytoplankton primary productivity. We evaluated the effects of the ~~subglacial upwelling-submarine discharge~~ on primary production in a seasonally fast ice covered Svalbard fjord (Billefjorden) influenced by a tidewater outlet glacier in April/May 2019. We found clear evidence for subglacial ~~upwelling~~discharge and upwelling. Although the estimated entrainment factor (1.6) and total fluxes were lower than in summer studies, we observed substantial impact on the fjord ecosystem and primary production. The subglacial meltwater leads to a salinity stratified surface layer and sea ice formation with low bulk salinity and permeability. The combination of the stratified surface layer, a two-fold higher under-ice irradiance, and higher N and Si concentrations at the glacier front supported two orders of magnitude higher primary production (42.6 mg C m⁻² d⁻¹) compared to a marine reference site at the fast ice edge. The nutrient supply increased primary production by approximately 30 %. The brackish water sea ice at the glacier front with its low bulk salinity contained a reduced brine volume, limiting the inhabitable place and nutrient exchange with the underlying seawater compared to full marine sea ice. Microbial and algal communities were substantially different in subglacial influenced water and sea ice compared to the marine reference site, sharing taxa with the subglacial outflow water. We suggest that with climate change, the retreat of tidewater glaciers in early spring could lead to decreased under-ice phytoplankton primary production, while sea ice algae production and biomass may become increasingly important, unless sea ice disappears before, in which case spring phytoplankton primary production may increase.

34 1 Introduction

35 Tidewater glacier fronts have recently been recognized as hotspots for marine production including top trophic levels, such as
36 marine mammals, birds and piscivorous fish (Lydersen et al., 2014, Meire et al., 2016**b**), but also primary producers (Meire et
37 al., 2016**b**; Hopwood et al., 2020). During summer, large amounts of freshwater are released below the glacier and entrap
38 nutrient rich bottom water, sediments and zooplankton during the rise to the surface (Meire et al., 2016**a**, Moon et al., 2018).
39 Together with katabatic winds pushing the surface water out of the fjords, ~~it~~ submarine discharge creates a strong upwelling
40 effect (Meire et al., 2016**a**). The biological response to this upwelling will depend on the characteristics of the upwelling water.
41 ~~The~~ Primary production is typically low in direct proximity to the glacier front (hundreds of meters to kilometres, Halbach et
42 al., 2019) due to high sediment loads of the plumes absorbing light ~~and thereby inhibit primary production close to the glacier~~
43 ~~front, but potentially also due to lateral advection (Meire et al., 2016ab; Halbach et al., 2019).~~ The light absorbing effect of
44 the plumes is highly dependent on the glacial bedrock (Halbach et al., 2019). However, the high nutrient concentrations
45 supplied to the surface increase summer primary production at some distance (hundreds of meters to kilometres, Halbach et
46 al., 2019) from the initial upwelling discharge event, once the sediments settled out (Meire et al., 2016, Halbach et al., 2019).
47 These tidewater upwelling effects have been described in a variety of different Arctic fjords including deep glacier termini in
48 western Greenland (Meire et al., 2016), eastern Greenland (Cape et al., 2019), and north-western Greenland (Kanna et al.,
49 2018), but also in shallower fjords on Svalbard (Halbach et al., 2019). Due to the challenges of Arctic field work in early spring
50 and the difficulties of locating such an outflow, only few studies investigated submarine discharge during that time window.
51 The few studies available suggest overall little discharge (e.g. Fransson et al., 2020; Schaffer et al., 2020) compared to summer
52 values. The limited amount of data makes the generalized quantification of subglacial outflow difficult. In addition, studies
53 focusing on the potential impacts of the early spring discharge on sea ice and pelagic primary production are lacking. Studies
54 of the effect of potential subglacial upwelling in winter/spring on sea ice and pelagic primary productivity are lacking due to
55 the perception of the absence of freshwater outflows in winter.
56
57 In addition to submarine discharge at the grounding line, tidewater glacier related upwelling mechanisms can also be caused
58 by the melting of deep icebergs (Moon et al., 2018), or the melting of the glacier terminus in contact with warm seawater
59 (Moon et al., 2018, Sutherland et al., 2019). A seasonal study within an East Greenland fjord showed high melt rates of icebergs
60 throughout the year ~~(Moon et al., 2018)~~, while subglacial runoff had been detected as early as April, but with substantially
61 higher freshwater inputs in summer: (Moon et al., 2018). Glacier terminus melt rates occurring at the glacier-marine interface
62 are low compared to the subglacial outflow but can be present throughout the year (Chandler et al., 2013, Moon et al., 2018).
63 In fact, Moon et al. (2018) found higher terminus melt rates below 200 m in winter than in summer, which may allow winter
64 upwelling. Submarine glacier termina on Svalbard ~~glaciers are occur~~ typically at shallower water depth than on Greenland and
65 deep terminus melt (below 200 m) and iceberg induced upwelling are less important (Dowdeswell, 1989). However, subglacial
66 outflows can persist through~~out~~ winter and ~~specifically in into~~ spring through the release of subglacial meltwater stored from

67 the previous summer and fall melt season as observed in several Svalbard glaciers, including cold-based glaciers (Hodgkins,
68 1997). ~~Hodgkins (1997) described the release of subglacial meltwater stored from the previous summer to fall melt season~~
69 ~~from various Svalbard glaciers, including cold-based glaciers.~~ Winter drainage occurred mostly periodically during events of
70 ice-dam breakage. During the storage period, the meltwater can change its chemical composition. For example, ~~During~~
71 ~~prolonged contact with silicon-rich bedrock, the meltwater becomes enriched in the~~ increased the ~~macronutrient~~-silicate
72 concentrations (Hodgkins, 1997). Additionally, ~~during~~ freezing of some of the meltwater leads ~~, solutes are expelled leading~~
73 ~~to higher ion concentrations in the remaining liquid fraction~~ (Hodgkins, 1997). Under polythermal glaciers, various
74 ~~other~~ additional mechanisms such as ~~constant~~ supply from groundwater, and basal ice melt via geothermal heat, pressure, or
75 frictional dissipation can also ~~be a continuous~~ contribute to a continuous, but low flux meltwater source in winter and spring
76 (Schoof et al., 2014). ~~or through constant supply from groundwater, temperate parts of the glacier, geothermal heat, or frictional~~
77 ~~dissipation~~ (Schoof et al., 2014). Sediment inputs into the fjord during this time of the year are low with peaks deeper in the
78 water column, indicating limited impacts on surface primary production (Moskalik et al., 2018). While studies on
79 ~~upwelling~~ glacial discharge in winter and spring are limited to oceanographic observations, (Fransson et al., 2020, Schaffer et
80 al., 2020), the biological effects on e.g. primary production have been neglected (Chandler et al., 2013, Moon et al., 2018).
81 ~~Even~~ We hypothesize that subglacial discharge can lead to significantly increased primary production, due to upwelling of
82 nutrient rich deeper water or through its own nutrient load, especially towards the end ~~-of the spring bloom.~~ low rates of
83 subglacial outflows can be sufficient to supply nutrients to the surface, while We suggest that during this time ~~A~~ at the same
84 time ~~considerably less light absorbing sediments are entrapped due to lower upwelling fluxes in~~ considerably less light
85 absorbing sediments compared to the summer situation (Moskalik et al., 2018).

86

87 ~~W~~ After light becomes available in spring ~~with the return of the sunlight after the polar night, Arctic ice algae and phytoplankton~~
88 ~~may start forming blooms fueled~~ sustained by the winter mixing replenished nutrients ~~supplied via winter mixing with different~~
89 onsets in different parts of the Arctic. The blooms are typically terminated by limitation of macronutrients, ~~either~~ mainly nitrate
90 or silicate (Leu et al., 2015). We suggest that in the absence of wind induced mixing, due to the seasonal presence of fast ice
91 cover in spring, submarine discharge of glacial meltwater can directly (nutrient ion enrichment over the subglacial storage
92 period) or indirectly (upwelling) be a significant source of inorganic nutrient ~~significantly increasing~~ primary production in
93 front of tidewater glaciers compared to similar fjords without these glaciers. Especially after nutrients supplied via winter
94 mixing are incorporated into algal biomass (Leu et al. 2015) this additional nutrient source may become important. Evaluating
95 this process is also relevant as ~~especially towards the end of the ice algal/phytoplankton spring bloom when nutrients become~~
96 limiting (Leu et al. 2015). ~~With~~ climate change ~~will substantially change~~, these dynamics ~~are expected to change substantially~~
97 (e.g. Błaszczyk et al., 2009, Holmes et al., 2019). Higher glacial melt rates and earlier runoffs may initially increase tidewater
98 glacier induced upwelling, ~~due to increased subglacial runoff~~ (Amundson and Carroll, 2018). However, their retreat and
99 transformation into ~~first~~ shallower tidewater glacier termini ~~with~~ may lead to less pronounced upwelling ~~and finally, unless the~~
100 shallower grounding line is compensated by the increased runoff (Amundson and Carroll, 2018). Eventually, the tidewater

~~glaciers transform~~ into land ~~terminated glaciers will eliminate the terminating glaciers, where wind induced mixing is still possible, but upwelling submarine discharge process—thus is eliminated (Amundson and Carroll, 2018) – potentially~~ reducing the primary production.

Due to high inputs of freshwater in the autumn preceding the onset of sea ice formation, tidewater glacier influenced fjords are often sea ice covered in spring, mainly by coastal fast ice. Within the sea ice, ice algae start growing, once sufficient light ~~is penetrating-penetrates~~ the snow and ice layers ~~with the onset varying, ice algae start growing within sea ice~~ between March and April, depending on latitude and local ice conditions (Leu et al., 2015). While the beginning of the ice algal blooms is typically related to light, the magnitude depends on the initial nutrient concentration and ~~advection of nutrient-rich seawater nutrient additions~~ from the water column into the brine channel network (Gradinger, 2009). Thus, ~~early spring~~ subglacial upwelling- has the strong potential to extend the duration and increase the magnitude of the ice algal blooms. Similar control mechanisms apply to phytoplankton bloom formation and duration. ~~Phytoplankton growth under sea ice is often light limited, and u~~Under-ice phytoplankton blooms ~~are thought to be light limited if the ice is snow covered and substantial blooms have~~ been described in areas with ~~increased under-ice light intensities due to e.g. the~~ lack of snow cover (e.g. melt ponds, after rain events, Fortier et al., 2002, Arrigo et al., 2014) or at the ice edge related to ~~ice edge wind-induced Ekman~~ upwelling (Mundy et al., 2009). On Svalbard, low precipitation rates and strong katabatic winds (Esau & Repina, 2012) often limit snow ~~coverage accumulation also~~ on the fast ice near glacier fronts (Braaten, 1997), potentially allowing enough light for under-ice phytoplankton blooms to occur. ~~We also suggest that the unique sea ice features could increase the under-ice light intensity. Sea ice formed from brackish water has a low bulk salinity, brine volume fraction and permeability (Golden et al., 1998) and resulting low total ice algal biomass as observed e.g. in the Baltic Sea (Haecky & Andersson, 1999). This lower algal biomass will reduce ice algal light absorption allowing more light to reach the under-ice phytoplankton. Once After With~~ sufficient light ~~reaches the water column,~~ typically a diatom dominated ~~phytoplankton~~ bloom starts along the receding ice edge or even below the sea ice (e.g. Hodal et al., 2012; Lowry et al., 2017). Once silicate becomes limiting for diatom growth, other taxa like *Phaeocystis pouchetii* dominate the next stage of the seasonal succession (von Quillfeldt, 2000). ~~These is algal~~ succession pattern ~~in ice and water column~~ can be significantly influenced by tidewater glacier ~~related-induced~~ spring upwelling. ~~Sea ice formed from brackish water has relatively low bulk salinity, low brine volume (Golden et al., 1998). and low total ice algal biomass as observed e.g. in the Baltic Sea (Haecky & Andersson, 1999). Sea ice with reduced bulk salinity has a reduced permeability compared to more saline ice at identical temperatures (Golden et al., 1998). Brackish ice conditions with low algal biomass will reduce light absorption allowing more light to reach the water column to potentially fueling under ice phytoplankton blooms.~~ We suggest that higher nutrient levels supplied via ~~slow~~ subglacial upwelling ~~of low total flux~~ in the absence of wind mixing may enhance algal growth ~~and cause different succession patterns for phytoplankton and sea ice algae.~~

135 We used the natural conditions in a Svalbard fjord as a model system contrasting the biological response at two glacier fronts
136 with ~~different freshwater input~~ only one glacier front supplying submarine freshwater discharge during the winter/spring (early
137 spring) transition period while a fast ice cover was present. The aim of the study was to investigate the effect of the glacier
138 terminus, and subglacial outflow related upwelling on the light and nutrient regime in the fjord and thereby on
139 winter/spring/early spring primary productivity and algae community structures both in and under the sea ice. We hypothesized
140 that; 1) subglacial upwelling-submarine discharge throughout winter and spring supplies nutrient rich glacial meltwater and
141 upwelling of marine bottom water to the surface, 2) subglacial upwelling-submarine discharge increases primary production
142 near the glacier front (< 500 m), 3) biomass of sea ice algae is lower at glacier fronts as a result of low permeability sea ice
143 limiting nutrient exchange and inhabitable space.

144

145 2 Methods

146 2.1 Field work and physical properties

147 Fieldwork was conducted on Svalbard in Billefjorden (Fig. 1) between 22nd of April and 5th of May 2019, when most of the
148 samples were collected. For comparison, ~~some additional~~ samples had been already taken in April 2018 (subglacial outflow
149 water for DNA analyses) and July 2018 (glacier ice and supraglacial runoff). Billefjorden is fed by a few streams, rivers and
150 the tidewater glacier Nordenskiöldbreen and partly fast ice covered from January to June. Nordenskiöldbreen has an estimated
151 grounding depth of 20 m at its southern margin (personal observation). Tidal currents are very slow with under 0.1 cm s⁻¹,
152 which translates to advection below 22 m per tidal cycle (Kowalik et al., 2015). Katabatic winds can be strong due to several
153 glaciers and valleys leading into the fjord system (Láska et al., 2012). Together with low precipitation, this leads to a thin snow
154 depth on the sea ice. Bare sea ice spots are often present in the sea ice season (personal observations). The fjord is separated
155 from Isfjorden, a larger fjord connected to the West Spitsbergen current, by a shallow ~~sill~~ approximately 30 to 40 m deep sill
156 (Norwegian Polar Institute, 2020) making Billefjorden an Arctic fjord with limited impacts of Atlantic water inflows. This
157 character is shown in water masses, circulation patterns and animal communities including the presence of polar cod (Maes,
158 2017, Skogseth et al., 2020).

159 Samples were taken at three stations 1) at the fast ice edge (IE) – a full marine reference station (78°39'09N, 16°34'01E); 2) at
160 the southern site of the ocean terminated glacier terminus (SG) (approx. 20 m water depth) with freshwater outflow observed
161 during the sampling period (78°39'03N, 16°56'44E) and; 3) at the northern site of the glacier terminus (NG) with no clear
162 freshwater outflow observed and a mostly land-terminating glacier front (78°39'40N, 16°56'19E).

163 Snow depth and sea ice thickness around the sampling area were measured with a ruler. Sea ice and glacier ice samples were
164 taken with a Mark II ice corer with an inner diameter of 9 cm (Kovacs Enterprise, Roseburg, OR, USA). Temperature of each
165 ice core was measured immediately by inserting a temperature probe (TD20, VWR, Radnor, PA, USA) into 3 mm thick pre-
166 drilled holes. For further measurements the ice cores were sectioned into the following sections: 0–3 cm, 3–10 cm and

167 thereafter in 20 cm long pieces from the bottom to the top, packed in sterile bags (Whirl-Pak™, Madison, WI, USA) and left
 168 to melt at about 4–15 °C for about 24–48 h in the dark. Sections for chlorophyll *a* (Chl) measurements, DNA extractions, and
 169 algae and bacteria counts were melted in 50 % vol/vol sterile filtered (0.2 µm Sterivex filter, Sigma-Aldrich, St. Louis, MO,
 170 USA) seawater, to avoid osmotic shock of cells (Garrison and Buck 1986), while no seawater was added to the sections for
 171 salinity and nutrient measurements. Salinity was measured immediately after melting using a conductivity sensor (YSI Pro 30,
 172 YSI, USA). Brine salinity and brine volume fractions were calculated after Cox et al. (1983) for sea ice temperatures below -
 173 2 °C and after Leppäranta and Manninen (1988) for sea ice temperatures above.
 174 Samples of under-ice water were taken using a pooter (Southwood and Henderson, 2000) connected to a hand-held vacuum
 175 pump (PFL050010, Scientific & Chemical Supplies Ltd., UK). Deeper water at 1 m, 15 m, 25 m depths and bottom water at
 176 IE station were taken with a water sampler (Ruttner sampler, 2 L capacity, Hydro-Bios, Germany). Glacial outflow water was
 177 sampled in April 2018 close to SG station using sterile Whirl-Pak™ bags. No outflow water was found around NG station.
 178 Cryoconite hole water (avoiding any sediment) was sampled in July 2018 with a pooter on sites known to differ in their
 179 biogeochemical settings (Nordenskiöldbreen main cryoconite site (NC), and Nordenskiöldbreen near Retrettøya (NR) sites
 180 characterized by Vonnahme et al., 2016). One m-thickmetre long glacier surface ice samples were taken with the Mark II ice
 181 corer at the southern side of the glacier on the NC site.
 182 CTD profiles were taken at each station by a CastAway™ (SonTek/-Xylem, San Diego, CA, USA). At the SG station an
 183 additional CTD profile was taken with a SAIV CTD SD208 (SAIV, Lakselv, Norway) including turbidity and fluorescence
 184 sensors. Unfortunately, readings at the other stations failed due to sensor freezing at low air temperatures. Surface light data
 185 were obtained from the photosynthetic active radiation (PAR) sensor of the ASW 1 weather station in Petuniabukta (23 m
 186 a.s.l), operated by the University of South Bohemia (Láska et al., 2012; Ambrožová and Láska, 2017).
 187 During the sampling days, Billefjorden and Adventdalen were overcast. The light regime under the ice was calculated after
 188 Masicotte et al. (2018) with a snow albedo of 0.78, a snow attenuation coefficient of 15 m⁻¹ (Mundy et al., 2005), ice attenuation
 189 coefficients of 5.6 m⁻¹ for the upper 15 cm and 0.6 m⁻¹ below (Perovich et al., 1998). For sea ice algae, an absorption coefficient
 190 of 0.0025 m² mg⁻¹ Chl was used. The fraction of fjord water vs subglacial meltwater for the water samples was calculated
 191 assuming linear mixing (Equations 1-2) of the two salinities (Meltwaterglacial meltwater salinity = 0 PSU, average seawater
 192 salinity at IE=34.6-PSU7 ± 0.03 standard deviation), since no other water masses in regard to temperature or salinity signature
 193 were present (Table 1). The variability of the IE seawater salinity leads to a small (0.1 %) uncertainty in the estimated value
 194 of the relative contributions of sea water vs subglacial meltwater.

195 **2.2 Chemical properties**

196 Nutrient samples of water and melted sea ice and glacier ice were sterile filtered as described above, stored in acid washed
 197 (rinsed in 5 % vol/vol HCl) and MQ rinsed 50 ml falcon tubes and kept at -20 °C until processing. Total alkalinity (TA),
 198 Dissolved inorganic carbon (DIC), and pH samples were sampled in 500 ml borosilicate glass bottles avoiding air
 199 contamination and fixed within 24 h with 2 % (fin. con.) HgCl₂ and stored at 4 °C until processing.

200 Nutrients were measured in triplicates using standard colorimetric methods with a nutrient autoanalyser (QuAatro 39, SEAL
201 Analytical, Germany) using the instrument protocols: Q-068-05 Rev. 12 for nitrate (detection limit = $0.02 \mu\text{mol L}^{-1}$), Q-068-
202 05 Rev. 12 for nitrite (detection limit = $0.02 \mu\text{mol L}^{-1}$), Q-066-05 Rev. 5 for silicate (detection limit = $0.07 \mu\text{mol L}^{-1}$), and Q-
203 064-05 Rev. 8 for phosphate (detection limit = $0.01 \mu\text{mol L}^{-1}$). The data were analysed using the software AACE v5.48.3
204 (SEAL Analytical, Germany). Reference seawater (Ocean Scientific International Ltd., United Kingdom) was used as blanks
205 for calibrating the nutrient analyser. The maximum differences between the measured triplicates were $0.1 \mu\text{mol L}^{-1}$ for silicate
206 and nitrate and $0.05 \mu\text{mol L}^{-1}$ for nitrite and phosphate. Concentrations of nitrate and nitrite (NO_x) were used to estimate the
207 fraction of bottom water reaching the surface at SG assuming linear mixing of subglacial meltwater, bottom water (at station
208 IE) and surface water concentration using the NO_x concentration measured at IE and the subglacial meltwater (Table 1). The
209 calculations for these mixing estimates are given in the appendix.
210 DIC and TA were analyzed within 6 months after sampling as described by Jones et al. (2019) and Dickson et al. (2007). DIC
211 was measured on a Versatile Instrument for the Determination of Titration carbonate (VINDTA 3C, Marianda, Germany),
212 following acidification, gas extraction, coulometric titration, and photometry. TA was measured with potentiometric titration
213 in a closed cell on VINDTA Versatile INstrument for the Determination of Titration Alkalinity, VINDTA 3S, Marianda,
214 Germany). Precision and accuracy was ensured via measurements of Certified Reference Materials (CRM, obtained from
215 Dickson, Scripps Institution of Oceanography, USA). Triplicate analyses on CRM samples showed mean standard deviations
216 below $\pm 1 \mu\text{mol kg}^{-1}$ for DIC and AT.

217 **2.3 Biomass and communities**

218 For determination of algal pigment concentrations about 500 ml sea water or melted sea ice were filtered onto GF/F filter
219 (Whatman plc, Maidstone, UK) in triplicates using a vacuum pump (max 200 mbar vacuum) before storing the filter in the
220 dark at -20°C . Water and melted sea ice for DNA samples were filtered onto Sterivex filter ($0.2 \mu\text{m}$ pore size) using a peristaltic
221 pump and stored at -20°C until extraction. Algae were sampled in two ways; 1) a phytoplankton net ($10 \mu\text{m}$ mesh size) was
222 pulled up from 25 m and the samples fixed in 2 % (final conc.) neutral Lugol and stored at 4°C in brown borosilicate glass
223 bottles before processing; and 2) water or melted sea ice was fixed and stored directly as described above. For later bacteria
224 abundance estimation, 25 ml of water was fixed with 2 % (final con.) formaldehyde for 24–48 h at 4°C before filtering onto
225 $0.2 \mu\text{m}$ polycarbonate filters (Isopore™, Merck, US) and washing with filtered seawater and 100 % ethanol before freezing at
226 -20°C .

227 Algal pigments (Chl, phaeophytin) were extracted in 5 ml 96 % ethanol at 4°C for 24 h in the dark. The extracts were measured
228 on a Turner Trilogy AU-10 fluorometer (Turner Designs, 2019) before and after acidification with a drop of 5 % HCl. 96 %
229 ethanol was used as a blank and the fluorometer was calibrated using a chlorophyll standard (Sigma S6144). For estimations
230 of algae derived carbon a conversion factor of $30 \text{ g C (g Chl)}^{-1}$ was applied (Cloern et al., 1995). The maximum differences
231 (max-min) between the measured triplicates were under $0.05 \mu\text{g Chl L}^{-1}$ unless stated otherwise.

232 DNA was isolated from the Sterivex filter cut out of the cartridge using sterile pliers and scalpels, using the DNeasy®
 233 PowerSoil® Kit following the kit instructions with a few modifications. Solution C1 was replaced with 600 µL
 234 Phenol:Chloroform:Isoamyl Alcohol 25:24:1 and washing with C2 and C3 was replaced with two washing steps using 850 µL
 235 chloroform. Before the last centrifugation step, the column was incubated at 55 °C for 5 min to increase the yield. For microbial
 236 community composition analysis, we amplified the V4 region of a ca. 292 bp fragment of the 16S rRNA gene using the primers
 237 (515F, GTGCCAGCMGCCGCGGTAA and 806R, GGACTACHVGGGTWTCTAAT, assessed by Parada et al., 2016). For
 238 eukaryotic community composition analyses, we amplified the V7 region of ca 100-110 bp fragments of the 18S rRNA gene
 239 using the primers (Forward 5'-TTTGTCTGTTAATTSCG-3' and Reverse 5'-GCAATAACAGGTCTGTG-3', assessed by
 240 Guardiola et al., 2015). The Illumina MiSeq PE library was prepared after Wangenstein et al. (2018).
 241 For qualitative counting of algal communities, the phytoplankton net-hauls and bottom sea-ice samples were counted under an
 242 inverted microscope (Zeiss Primovert, Carl Zeiss AG, Germany) with 10x40 magnification. For quantitative counts, 10-50 ml
 243 of the fixed water samples were settled in an Utermöhl chamber (Utermöhl, 1958) and counted. Algae were identified using
 244 identification literature by Tomas (1997), and Throndsen et al. (2007). For bacteria abundance estimates, bacteria on
 245 polycarbonate filter samples were stained with DAPI (4,6-diamidino-2-phenylindole) as described by Porter and Feig (1980),
 246 incubating the filter in 30 µl DAPI (1 µg ml⁻¹) for 5 min in the dark before washing with MQ and ethanol and embedding in
 247 Citifluor:Vectashield (4:1) onto a microscopic slide. The stained bacteria were counted using an epifluorescence microscope
 248 (Leica DM LB2, Leica Microsystems, Germany) under UV light at 10x100 magnification. At least 10 grids or 200 cells were
 249 counted. The community structure of the phytoplankton net haul was used for estimating the contribution of sea ice algae to
 250 the settling community based on typical Arctic phytoplankton (Von Quillfeldt, 2000) and sea ice algal species (von Quillfeldt
 251 et al., 2003) described in literature.

252 **2.4 In situ measurements and incubations**

253 Vertical algal pigment fluxes were measured using custom made (Faculty of Science, Charles University, Prague, Czech
 254 Republic) short-term sediment traps (6.2 cm inner diameter, 44.5 cm height) at 1 m, 15 m, and 25 m under the sea ice anchored
 255 to the ice at SG and IE, as described by Wiedmann et al. (2016). Sediment traps were left for 24 h at the SG station and 37 h
 256 at the IE station. After recovery, samples for algal pigments were taken, fixed and analysed as described above. Vertical export
 257 was calculated as described in equation 7.

258 Primary production (PP) was measured based on ¹⁴C-DIC incorporation. Samples were incubated *in situ* in 100 ml polyethylene
 259 bottles attached to the rig of the sediment trap giving identical incubation times. Seawater or bottom sea ice melted in filtered
 260 seawater (ca 20 °C initial temperature to ensure fast ice melt) on site were incubated with ¹⁴C sodium bicarbonate at final
 261 concentration of 1 µCi ml⁻¹ (PerkinElmer Inc., Waltham, USA). PP samples were incubated in triplicates for each treatment
 262 with two dark controls for the same times as the sediment traps. Samples were filtered onto precombusted Whatman GF/F
 263 filters (max 200 mbar vacuum) and acidified with a drop of 37 % fuming HCl for 24 h for removing remaining inorganic
 264 carbon. The samples were measured in Ultima Gold™ Scintillation cocktail on a liquid scintillation counter (PerkinElmer Inc.,

Waltham, USA, Tri-Carb 2900TR) and PP was calculated after Parsons et al., (1984). Dark carbon fixation (DCF) rates were used to estimate bacterial biomass production using a conversion factor of 190 mol POC (mol CO₂)⁻¹ fixed (Molari et al., 2013).

For testing the effect of the water chemistry on phytoplankton growth, we designed a reciprocal transplant primary production experiment where the phytoplankton communities at SG and IE (1 m and 15 m) each were transplanted into the sterile filtered water of both SG and IE. 50 ml of the water containing the respective original phytoplankton community were transferred into 50 ml sterile filtered (0.2 µm) seawater of SG or IE each in 100 ml polyethylene bottles. The bottles were then incubated *in situ* at the appropriate original depth and primary production measured as described above. The aim of the experiment is to test if water chemistry alone is sufficient to increase primary production, or if the different differences in algal communities, light regimes, or temperatures are more important. A reciprocal transplant experiment was conducted in water from 1 m and 15 m depth under the sea ice to test for fertilizing effects of glacial front water at stations SG and IE. At each site, incubations were made where half of the initial water volume was replaced with sterile filtered (0.2 µm) seawater of either the same station or the other station, excluding physical effects (light, temperature, sediment load). These samples were incubated and processed together with the other PP incubations at the adequate depths as described above.

2.5 Statistics and bioinformatics

Silicate, phosphate and NO_x concentrations were plotted against salinities and correlation were tested via linear regression analysis using the lm function in R (R Core Team, Vienna, Austria). P values were corrected for multiple testing using the false discovery rate. Since the primary production estimates of the reciprocal transplant experiments were not normally distributed, came from a nested design, and had heterogeneous variance, a robust nested Analysis of variance (ANOVA) was performed to test for significant treatment effects of incubation water with water depth as nested variable. The map (Fig. 1) was created in R using the PlotSvalbard v0.9.2 package (Vihtakari, 2020). The Svalbard basemap was retrieved from the Norwegian Polar institute (2020, CC BY 4.0 license), the pan-Arctic map was retrieved from Natural Earth (2020, CC Public domain license), and the bathymetric map was retrieved from the Norwegian mapping authority (Kartverket, 2020, CC BY 4.0 license).

16S sequences were analysed using a pipeline modified after Atienza et al. (2020) based on OBITools v1.01.22 (Boyer et al., 2014). The raw reads were demultiplexed and trimmed to a median phred quality score minimum of 40 and sequence lengths between 215 bp and 299 bp (16S rRNA) or between 90 bp and 150 bp (18S rRNA) and merged. Chimaeras were removed using uchime with a minimum score of 0.9. The remaining merged sequences were clustered using swarm (Mahe et al., 2014). 16S swarms were classified using the RDP classifier (Wang et al., 2007) and 18S swarms using the sina aligner (Pruesse et al., 2012) with the silva SSU 138.1 database (Quast et al., 2012). Further multivariate analyses were done in R using the vegan package. The non-metric multidimensional scaling (NMDS) plots are based on Bray-Curtis dissimilarities of square root transformed and double Wisconsin standardized OTU tables and were used to visualize differences between groups (brackish

297 water at SG – Fjord water, sea ice – seawater). Analysis of Similarities (ANOSIM) were done to test for differences of the
298 communities between the groups (999 permutations, Bray-Curtis dissimilarities).

299 3 Results

300 3.1 Physical parameters

301 The physical conditions of sea ice (temperature T/bulk salinity S, [Fig. 2a, b](#)) and surface water (uppermost 4 m under the sea
302 ice, T and S, [Fig. 2c,d](#)) at the freshwater inflow impacted site SG differed substantially from NG and IE. The sea ice and the
303 upper 4 m under the sea ice ~~were having had~~ consistently lower salinities (<8 PSU) and higher temperatures (-0.4 °C to -0.2
304 °C) at SG compared to NG and IE and also compared to the deeper water masses at SG (salinity > 34.6 PSU, temperature < -
305 1.4 °C)([Fig. 2c,d](#)). Sea ice melt was unlikely because the measured water temperatures and sea ice temperatures were below
306 freezing point considering the sea ice bulk salinity. The water column at SG was highly stratified with a low salinity 4 m thick
307 layer under the sea ice, separated by a sharp ca 1 m thick pycnocline ([Fig. 2c,d](#)). In contrast, the water column at IE was fully
308 mixed and at NG only a minor salinity drop from 34.6 to 33.6 PSU occurred within the the upper 50 cm under the sea ice ([Fig.](#)
309 [2c,d](#)). Sea ice temperature and salinity showed similar variations between the three sites with SG ice having lower salinities
310 and higher temperatures relative to sea ice at the other stations ([Fig. 2a,b](#)). At SG, bulk salinities were mostly below 0.7 PSU
311 and calculated brine salinities below 14 PSU, except for the uppermost 40 cm where bulk salinities reached around 1.5 PSU
312 and a brine salinity of 32 PSU ([Fig. 2](#)). This resulted in very low brine volume fractions below 5 %, except for the lowermost
313 10 cm with brine volume fractions up to 9 % (Supplementary table S1). At IE and NG, bulk salinities are mostly above 5 PSU
314 (>40 PSU brine salinity) and temperatures were below -0.4 °C, which led to brine volume fractions above 6 % in all samples
315 and above 10 % in the bottom 30 cm.

316 The homogenous temperature and salinity water column profiles at IE and NG stations indicate the presence of only one water
317 mass (Local Arctic water, Skogseth et al., 2020). The only additional water mass was subglacial meltwater (salinity of 0 PSU)
318 mixed into the surface layer of SG. Applying a simple mixing model based on the two salinities (IE= 34.6 PSU, Glacier= 0
319 PSU) provide an estimation of the fraction of glacially derived water in the surface layer of ca. 85 % in the uppermost 2 m
320 under the sea ice, before decreasing to 0 % at 4 m under the sea ice below the strong halocline. The water sample taken 1 m
321 under the sea ice had a fraction of 32 % glacial meltwater (Table 1). For NG, glacial derived water contributed only 3 % in the
322 first 50 cm under the sea ice.

323

324 The SG station was 33 m deep and about 180 m away from the glacier front. The sea ice was 1.33 m thick and covered by 3
325 cm of snow. The ice appeared clear with some minor sediment and air bubble inclusions and missed a skeletal bottom layer.
326 In the water column, a higher potential sediment load was observed as a turbidity peak at the halocline ([Fig. 3](#)). Direct evidence
327 of subglacial outflow had been observed at the southern site of the glacier in form of icing and liquid water flowing onto the
328 sea ice in April 2018, April 2019 and October 2019 ([Fig. S4](#)), but this form of subglacial outflow froze before reaching the

329 fjord, which was additionally blocked by sea ice. The sea ice temperature was between -0.4 °C at the bottom and -1.7 °C at the
 330 top (Fig. 2b).

331 NG was 27 m deep and about 360 m away from the glacier front. The sea ice was thinner (0.92 m) and the snow cover thicker
 332 (6 cm) compared to SG. The ice had a well developed skeletal layer at the bottom with brown coloration due to algal biomass.
 333 The ice temperature ranged between -2 °C at the bottom to -2.7 °C at the top (Fig. 2b). The IE station was about 75 m deep
 334 and 50 m away from the ice edge. The sea ice was thinnest (0.79 m) and the snow cover thickest (10 cm). Sea ice temperatures
 335 were coldest ranging from -2.2 °C at the bottom to -3.1 °C on the top (Fig. 2b). Loosely floating ice algae aggregates were
 336 present in the water directly under the ice. The recorded surface PAR irradiance were similar during the primary production
 337 incubation times at SG and IE (SG: average=305 $\mu\text{E m}^{-2} \text{s}^{-1}$, min=13 $\mu\text{E m}^{-2} \text{s}^{-1}$, max=789 $\mu\text{E m}^{-2} \text{s}^{-1}$; IE: average=341 $\mu\text{E m}^{-2}$
 338 s^{-1} , min=37 $\mu\text{E m}^{-2} \text{s}^{-1}$, max=909 $\mu\text{E m}^{-2} \text{s}^{-1}$). Using published attenuation coefficients irradiance directly under the ice was 5
 339 $\mu\text{E m}^{-2} \text{s}^{-1}$ at IE and higher at SG with 9 $\mu\text{E m}^{-2} \text{s}^{-1}$ due to the thinner snow cover.

340 3.2 Nutrient variability in sea ice and water

341 ~~Subglacial outflow water and glacial ice had relatively low nutrient levels (in glacial ice: $\text{Si(OH)}_4 < 0.3 \mu\text{mol L}^{-1}$, $\text{NO}_x < 0.9 \mu\text{mol L}^{-1}$, $\text{PO}_4 < 0.875 \mu\text{mol L}^{-1}$, in outflow: $\text{Si(OH)}_4 < 1.5-2.0 \mu\text{mol L}^{-1}$, $\text{NO}_x 1.8-2.3 \mu\text{mol L}^{-1}$, $\text{PO}_4 < 0.1$~~
 342 ~~$\mu\text{mol L}^{-1}$).~~ ~~but~~ ~~the nutrient concentrations in subglacial outflow water were higher than in most sea ice samples and the~~
 343 ~~nutrient depleted surface water (1 m under the sea ice) at the station IE. Overall, Nutrient concentrations in the fjord were~~
 344 ~~highest in the bottom water (4.0- 4.5 $\mu\text{mol L}^{-1}$ Si(OH)_4 , 9.1- 9.6 $\mu\text{mol L}^{-1}$ NO_x , 0.7-0.8 $\mu\text{mol L}^{-1}$ PO_4) and depleted at the~~
 345 ~~surface and in the sea ice, with the exception of the under-ice water (UIW, 0- 1 cm under the sea ice) of SG, where NO_x (10~~
 346 ~~$\mu\text{mol L}^{-1}$) and silicate (19 $\mu\text{mol L}^{-1}$) levels were exceptionally high (Fig. 4). We cannot exclude anomalies or sampling~~
 347 ~~artifacts to be responsible for the high values supported only from XXX sample (triplicate measurement of one sample~~
 348 ~~collected, and therefor decided to used the values measured 1 m under the sea ice for further calculations in this manuscript as~~
 349 ~~surface water reference.~~ SG had overall higher levels of silicate and NO_x compared to ~~the~~ IE at both 1 m below the sea ice (by
 350 factors of 3 for Si(OH)_4 and 2 for NO_x) and bottom ice (by factor of 18 for Si(OH)_4 and 3 for NO_x compared to IE bottom
 351 ice) (Fig. 4). Silicate concentrations deeper in the water column were similar at all the stations with values of ca 4 $\mu\text{mol L}^{-1}$.
 352 Close to the surface silicate was reduced to 1.6 $\mu\text{mol L}^{-1}$ at 1 m at the IE, while it stayed at 4.3 $\mu\text{mol L}^{-1}$ at SG (Fig. 4a). In the
 353 water column, NO_x and phosphate gradients were similar between the sites. However in sea ice, NO_x concentrations were
 354 more than two times higher at SG than at the IE. In the bottom 30 cm of sea ice all nutrients had higher concentrations at SG,
 355 except for phosphate, which was depleted in the bottom 3 cm of SG, but not in the bottom of IE sea ice. In the ice interior in
 356 50- 70 cm distance from the ice bottom, also the other nutrients were depleted at SG, before rising slightly towards the surface
 357 of the ice. N:P ratios were generally highest at SG with values above 40, exceeding Redfield ratios in the surface water and
 358 sea ice. N:P ratios at the IE were below Redfield in the entire water column and bottom sea ice with values ranging from 10 to
 359 13. A slight increase in NO_x was observed at the sea ice-atmosphere interface at NG and SG. ~~Subglacial outflow water and~~
 360 ~~glacial ice had relatively low nutrient levels (in glacial ice: $\text{Si(OH)}_4 < 0.3 \mu\text{mol L}^{-1}$, $\text{NO}_x < 0.9 \mu\text{mol L}^{-1}$, $\text{PO}_4 < 0.75 \mu\text{mol L}^{-1}$~~
 361 ~~$\mu\text{mol L}^{-1}$).~~

⁺, in outflow: $\text{Si(OH)}_4 < 1.5 - 2.0$, $\text{NO}_x < 1.8 - 2.3 \mu\text{mol L}^{-1}$, $\text{PO}_4 < 0.1 \mu\text{mol L}^{-1}$), but the nutrient concentrations in subglacial outflow water were higher than in most sea ice samples and the depleted surface water (1 m under the sea ice) at the IE.

Nutrient versus salinity profiles can give indications of the endmembers (sources) of the nutrients (Fig. 5) ~~with based on a linear correlation being indicative of conservative mixing.~~ A positive correlation ~~for example would indicate conservative mixing (assuming high salinity indicates higher concentrations of the nutrients of in the saline~~ Atlantic water endmember ~~had,~~ while a negative correlation points to a higher concentrations ~~than melt water) in the fresh glacial meltwater endmember.~~ Biological uptake and remineralisation ~~as well as physical processes, such as external inputs by meltwater could inverse or weaken or~~ eliminate the correlation, indicating non-conservative mixing. In the water column at NG and IE, silicate ($R^2=0.66$, $p=0.008$), NO_x ($R^2=0.62$, $p=0.01$) and phosphate ($R^2=0.69$, $p=0.005$) showed conservative positive mixing patterns with higher contributions of Atlantic Wwater (Fig. 5a-c). At SG silicate was negatively correlated to salinity showed a negative correlation for silicate pointing to a higher contribution concentration of in glacial meltwater ($R^2=0.86$, $p<0.0001$). The absence of but not positive relations correlations for NO_x and PO_4 indicate non-conservative mixing pointing towards the relevance of biological uptake and release -measurements (Fig. 5d-f). At SG, silicate concentrations were higher with lower salinities. The same pattern was observed in sea ice, scaled to brine salinities, with higher silicate and NO_x concentrations in the fresher SG ice, compared to NG and IE (Fig. 5g-i). However, the R^2 value were lower in particular for Si(OH)_4 (NO_x : $R^2=0.18$, $p=0.059$; Si(OH)_4 : $R^2=0.41$, $p=0.002$).

The contribution of nutrients by upwelling as well as freshwater inflow from glacial meltwater was estimated by linear mixing calculations for the water layer 1 m below the sea ice, avoiding the potential outlier values directly under the ice (Eqs. 1-6). At 1 m below the sea ice, about 32 ± 0.1 % of the water was derived from glacial meltwater based on salinity-based mixing of glacial meltwater and local Arctic water (Table 1, Eq. 1-2). The remaining 68 % came from either bottom water upwelling (25 m at SG as reference) or entrained surface water (IE values at 1 m under the sea ice as reference). Based on a similar estimation for inorganic nutrients, 58 ± 1 % of NO_x and 48.49 ± 3 % of PO_4 was provided by subglacial upwelling (Table 1). For silicate, higher concentrations were required in the bottom water of subglacial meltwater at the glacier front to explain the very high surface concentrations measured. Considering the estimated NO_x and PO_4 fractions, the overall fraction of nutrients derived from upwelling was about 53 %. The overall budget 1 m under the sea ice is was 32 ± 0.1 % glacial meltwater, 53 ± 3 % subglacial upwelling (deep-marine bottom water), and 15 ± 3 % horizontal transport (surface water).

3.3 Carbon cycle

Net primary productivity (NPP) was overall one order of magnitude higher at SG than at IE, with the highest production value occurring within the brackish layer under the ice at SG ($5.27 \text{ mg m}^{-3} \text{ d}^{-1}$, Fig. 6, 7). Within this layer, also Chl values were about two times higher compared to IE (21 mg m^{-3} at SG, 9.1 mg m^{-3} at IE), and also the Chl-specific productivity in this layer exceeded values at the other stations (Table 2). Within sea ice, a slightly different pattern emerged. While the primary

395 productivity in the bottom sea ice (0–3 cm) was two times higher at SG compared to IE, Chl values were two order of
396 magnitudes lower (Fig. 6). This indicates high Chl-specific production at SG (5.6 mg C mg Chl d⁻¹ in the sea ice and 11.4 mg
397 C mg Chl d⁻¹ integrated over 25 m depth). At the IE, the contribution of released ice algae to algal biomass in the water column
398 was higher and the overall vertical Chl flux was about 1.5 times higher than at SG at 25 m depth. Bacterial biomass was
399 comparable at both stations with higher biomass concentrations within the ice than in the water column. Bacterial activity
400 (based on DCF) was comparable in the bottom sea ice at the two sites; however, it was 63x higher in the brackish surface water
401 of SG leading to very high growth rate estimates (Table 2) of 6 mg C m⁻³ d⁻¹.

402
403 Integrated Chl values over the uppermost 25 m of the water column were nearly identical for SG and IE with values of about
404 3.75 mg Chl m⁻² (Table 2). The fraction of Chl was highest at IE (85 %) and lowest at the SG (30 %) (Table 2). The integrated
405 NPP was considerably higher at SG (42.6 mg C m⁻² d⁻¹ at SG, 0.2 mg C m⁻² d⁻¹ at IE), while the vertical export of Chl was
406 about three times higher at IE than SG. This leads to more (14 times) vertical export based on the sediment trap measurements
407 than production at IE and considerably lower (5 %) export than production at SG (Table 2). Relative to the standing stock
408 biomass of Chl at IE, 0.2 % of the Chl was renewed daily by NPP at IE and 3 % was vertically exported daily at IE, which
409 would relate - assuming absence of ~~grazing and~~ advection – a daily loss of 3 % of the standing stock Chl. At SG, 38 % was
410 renewed per day, while 2 % were exported. As grazing was not estimated in this study, the suggested loss terms of Chl-a based
411 on the sediment trap data are likely underestimations. This leads to an accumulation of biomass of 38 % per day, and a doubling
412 time of about 2.6 days. Bacterial growth doubling times were estimated to be between minutes (SG water) and days (IE water),
413 but within hours in sea ice (Table 2).

414
415 Considering the N demand based on the carbon based PP measurement (16 mol C mol N⁻¹ after Redfield, 1934), about 2 µmol
416 N L⁻¹ month⁻¹ (equivalent to 32 % of 1 m value for NO_x) was needed to sustain the PP measured at SG. Assuming constant PP
417 and steady state nutrient conditions, 32 % of the surface water had to be replaced by subglacial upwelling per month to supply
418 this N demand via upwelling. Since only 62 % of the upwelling water was entrained bottom water the actual vertical water
419 replenishment rate would be 52 % per month. Assuming a 2 m freshwater layer under the ice, this translates to flux of about
420 1.1 m³ m⁻² month⁻¹. Considering the distance of 250 m to the glacier front and a width of 1.6 km of the SG bay, this translates
421 to a minimum of about 422,000 m³ month⁻¹.

422 The reciprocal transplant experiment aimed to show the effect of water chemistry on primary production in the absence of
423 effects related to different communities, temperature, or light. The results ~~from the reciprocal transplant experiment~~ (Fig. 7)
424 showed clearly that the higher NPP at SG, compared to NG was related to the ambient nutrient concentrations (nested ANOVA,
425 p=0.0038, F=10.88). In any combination, sterile filtered water from the SG had a fertilising effect on both SG and IE
426 communities, increasing PP of IE communities by approx. 30 %. SG communities of the most active fresh surface layer (1m)
427 fixed twice as much CO₂ when incubated in the same water, compared to incubations in the IE water.

3.4 Bacterial, archaeal and eukaryotic communities

After bioinformatic processing 13,043 bacterial and archaeal (16S rRNA) OTUs, belonging to 1,208 genera with between 9,708 and 331,809 reads were retained. Differences between the bacterial 16S sequences of the various sample types indicated that they can be used as potential markers for the origin of the water (Fig. 8). Sea ice and water communities were clearly separated The first non-metric multidimensional scaling (NMDS1) axis separated sea ice from water communities (ANOSIM, $p=0.004$, $R=0.35$) with no overlapping samples (Fig. 8a). Generally IE and NG communities were very similar, while sea ice and under-ice water communities at SG were significantly different (ANOSIM, $p=0.001$, $R=0.593$) from the other fjord samples. The second NMDS2 axis The NMDS showed also separation of 16S communities along a gradient from subglacial communities towards fjord communities, with SG communities being in between fjord and subglacial communities (Fig. 8a). Bacterial communities at SG in the bottom layer of the sea ice and the brackish water layer were more similar to subglacial outflow communities than the other samples in both 2018 and 2019. Six OTUs were unique to the glacial outflow and SG surface (closest relatives: *Fluviimonas*, *Corynebacterineae*, *Micrococcinae*, *Hymenobacter*, *Dolosigranum*), which are 6.6 % of their OTUs. The community structure of supraglacial ice samples was very different from any other sample. Also in the most abundant genera clear differences can be detected (Fig. S1). *Flavobacterium* sp. was most abundant in sea ice and UIW samples in both 2018 and 2019 at SG, but rare or absent in the other samples. *Aliiglaciecola* sp. was characteristic for NG sea ice and UIW samples. *Paraglaciecola* sp. was abundant in NG and IE sea ice and UIW samples, and *Colwellia* sp. was abundant in all sea ice and UIW samples. In sea water samples the genus *Amphritea* sp. was more abundant. *Pelagibacter* sp. was abundant in all samples. Glacial outflow water was dominated by *Sphingomonas* sp. and glacier ice by *Halomonas* sp., which were rare or absent in the other samples.

The eukaryotic community (18S rRNA) consisted of 4,711 OTUs, belonging to 535 genera, with between 2,204 and 15,862 reads. Overall, the same NMDS clustering has been found as for the 16S rRNA sequencing. We found distinctive communities in the sea ice and 1 m layer under the sea ice at SG being significantly different (ANOSIM, $p=0.001$, $R=0.456$) to the other samples (Fig. 8c). In fact, the SG surface communities were more similar to the outflow community (Fig. 8c). The clear differentiation between all sea ice and water column communities was also visible in the 18S rRNA samples (ANOSIM, $p=0.005$, $R=0.192$). As for the 16S communities, also the abundant genera differed between the groups (Fig. S2). The cryptophytes *Hemiselmis* sp. and Geminigeraceae were abundant at SG, but rare at the other sites. Dinophyceae, Imbricatea (*Thaumatomastix* sp.) and Bacillariophyceae were abundant in all samples with diatoms being mostly more abundant in sea ice or UIW. The Chytridiomycota family of Lobulomycetaceae were abundant in water samples from 2018, but not 2019. Subglacial outflow water was dominated by unclassified Cercozoa and *Bodomorpha* sp..

In total 22 different taxa were detected by microscopy. The community composition was clearly separated between sea ice and water samples. Furthermore sea ice species-algal composition at SG station differed from NG and IE (Fig. 8cb). SG sea ice was completely dominated by unidentified flagellates (potentially *Hemiselmis* sp., Geminigeraceae, and *Thaumatomastix* sp. based on 18S sequences), with the exception of the 70–90 cm layer with high abundances of *Leptocylindrus minimus*. Sea

ice samples at NG and IE were dominated by the typical Arctic ice algae *Navicula* sp. and *Nitzschia frigida*. Water samples were more diverse with abundances of *Fragillariopsis* sp., *Coscinodiscus* sp., and *Chaetoceros* sp.. Overall, diatoms dominated most samples at NG and IE in sea ice and water samples.

4 Discussion

The hydrography, sea ice properties, water chemistry and bacterial communities at SG provide clear evidence for ~~subglacial upwelling-submarine discharge and upwelling~~ at a shallow tidewater outlet glacier under sea ice, a system previously not considered for subglacial upwelling processes. Briefly, our first hypothesis that ~~subglacial upwelling-submarine discharge~~ persists also in ~~winter/spring~~ early spring, supplying nutrient-rich glacial meltwater and upwelling of bottom fjord water to the surface has been confirmed as discussed in detail below.

4.1 Indications for ~~subglacial-submarine discharge and~~ upwelling

The physical properties at SG were distinctly different to stations NG and IE. In contrast to NG and IE, the marine terminating SG site had a brackish surface water layer of 4 m thickness under the sea ice and low sea ice bulk salinities below 1.5 PSU comparable to sea ice in the nearby tidewater glacier influenced Tempelfjorden (Fransson et al., 2020) and in brackish Baltic sea ice (Granskog et al., 2003). We excluded surface melt or river run off as freshwater sources for the following reasons. With air temperatures below freezing point during the sampling periods, surface runoff based on snowmelt was not possible and no melting was observed during field work. In addition, no major river flow into the main bay studied (Adolfbukta), as indicated by small catchment areas (Norsk Polarinstitutt, 2020). We did observe some subglacial runoff at the southern site of the glacier (close to SG), ~~however but~~ this outflow water froze before it reached the fjord, which was additionally blocked by a 1.33 m thick sea ice cover. The sea ice cover would also block any inputs by atmospheric precipitation, considering the impermeable sea ice conditions especially at SG with brine volume fractions below 5 % (Golden et al., 1998; Fransson et al., 2020). Additional potential freshwater sources could be related to ~~basal-glacial terminus~~ ice melt of glacier fronts (Holmes et al., 2019; Sutherland et al., 2019) or icebergs (Moon et al., 2018). However, in the absence of Atlantic water inflow, which is blocked in Billefjorden by a shallow sill depth at the entrance of Billefjorden (Skogseth et al., 2020), water temperatures were consistently below freezing point (~~max -0.2 °C~~) and no Atlantic inflow water was detected at any station. ~~These low water temperatures which~~ does not allow ~~basal-glacial~~ glacier terminus ice to melt in Billefjorden. ~~Subglacial meltwater itself is unlikely to lead to basal ice melting due to its low salinity.~~ However, basal-glacier terminus ice melt is likely more important in systems with Atlantic water inflows, such as Greenland or Svalbard fjords without a shallow sill (e.g. Kongsfjorden and Tunabreen, Holmes et al., 2019). Sea ice may melt at lower temperatures compared to glacial ice, but the absence of typical sea ice algae in the water column at SG and the low salinity of the sea ice indicated that this was not the case. In fact, sea ice with a salinity of 1.5 PSU (measured at SG) would melt at -0.08 °C (Fofonoff et al., 1983), but the water and ice temperatures did not exceed -0.2 °C. Consistent with our study Fransson et al. (2020) also found substantial amount of freshwater in the sea

ice in Tempelfjorden (approx. 50 % meteoric water fraction) in a year with large glacier meltwater contribution further supporting the presence of ~~subglacial upwelling-submarine discharge~~ under sea ice. Fransson et al. (2020) suggested the combination of low salinities with high silicate concentrations as indicator for glacial meltwater, which was also the case in our study. In addition, the overall low sea ice ~~bulk~~ salinity and sediment inclusions at SG cannot be explained by sea ice melt, but must originate from another source. Clear evidence for outflow comes also from the visual observations of subglacial outflow exiting the land-terminating part south of the glacier in October 2019, April 2018 and April 2019, which we assume also occurred under the marine terminating front. In fact, subglacial outflows in spring have been observed at various other Svalbard glaciers with runoff originating from meltwater stored under the glacier from the last melt season and released by changes in hydrostatic pressure or glacier movements (Wadham et al., 2001). Active subglacial drainage systems in winter have also been described elsewhere; and can be sustained by geothermal heat or frictional dissipation, groundwater inputs, or temperate ice in the upper glacier (Wilson 2012; Schoof et al., 2014). This meltwater has also been found to be rich in can have silicate concentrations due to the long contact with the subglacial bedrock during its storage over winter (Wadham et al., 2001; Fransson et al., 2020). We therefore suggest that early spring submarine discharge is not unique to Billefjorden, but likely occurs at all polythermal or warm based marine-terminating glaciers.

4.2 Potential magnitude of ~~subglacial-submarine discharge and~~ upwelling

Considering the slow tidal currents in our study area (<22 m per 6 h tidal period, Kowalik et al., 2015) and wind mixing blocked by sea ice, a potential source of the freshwater within Billefjorden may be ~~meltwater introduced during the last summer to fall melting season and remaining throughout winter, remains from the previous melting season~~. Hence, the question of how much subglacial meltwater reaches the surface at SG is important. We estimated that the fresh surface water was most likely exchanged on time scales of days to weeks. Even slow vertical mixing would be capable to erode the halocline in over six months since the last melting season. The turbidity peak we observed at the halocline would also settle out in a short time (weeks), if not replenished by fresh inputs (Meslard et al., 2018). Vertical export flux was determined to account for approximately 4% of the Chl standing stock at 25 m. Considering that glacial sediment settles typically substantially faster than phytoplankton due its higher density this suggests that the turbidity peak would erode within days to weeks without fresh sediment input via upwelling (Meslard et al., 2018). Furthermore, the inorganic nitrogen demand for the measured primary productions would consume the present nutrients in a few (approx. 2) months. Assuming steady state, the nutrient uptake by phytoplankton primary production would require an upwelling driven water flux of at least $1.1 \text{ m}^3 \text{ m}^{-2} \text{ month}^{-1}$. Microbial communities (16S rRNA and 18S rRNA) in SG UIW and sea ice were similar to the subglacial outflow water. Bacterial communities (16S rRNA) at SG shared 6.6 % of their OTUs with subglacial outflow communities, which is twice as much as NG and IE (3.6 %) shared with the outflow communities. Considering the estimated bacterial ~~growth rates~~ production and biomass (Table 2) at SG the doubling time of the bacteria would be between 0.5 h and 7 h (Table 2). However, the use of a conversion factor for biomass production based on sediment bacterial data is adding uncertainty to the estimation of the bacterial doubling time. Estimates reported from Kongsfjorden in April are indeed longer (3-10 days, Iversen & Seuthe, 2010),

as are other Arctic bacterioplankton doubling time estimates ranging between 1.2 days (Rich et al., 1997), 2.8 days (de Kluijver et al., 2013) and weeks (2 weeks, Rich et al., 1997; 1 week, Kirchman et al., 2005).

Based on the growth in the range of hours to days, the distinctive community at SG would have changed to a more marine community on time scales of weeks, assuming only growth of marine OTUs at SG and settling out or grazing of inactive glacial bacteria taxa. Thus, we suggest that ~~Consequently,~~ the presence of shared OTUs between SG and the glacial outflow may indicates a constant-continuous supply of fresh inoculum to sustain these taxa. ~~The clearest evidence for outflow comes from the visual observations of subglacial outflow exiting the southern part of the glacier in October 2019, April 2018 and April 2019 which we assume also occurred under the marine terminating front. In fact, subglacial outflows in spring have been observed at various other Svalbard glaciers with runoff originating from meltwater stored under the glacier from the last melt season and released by changes in hydrostatic pressure or glacier movements (Wadham et al., 2001). Active subglacial drainage systems in winter have also been described elsewhere, and can be sustained by geothermal heat or frictional dissipation, groundwater inputs, or temperate ice in the upper glacier (Wilson 2012; Schoof et al., 2014). This meltwater has also been found to be rich in silicate due to the long contact with the subglacial bedrock during its storage over winter (Wadham et al., 2001; Fransson et al., 2020). Overall, our marine evidence bybased on salinity and nutrient profiles, turbidity, and communities support the occurrence of submarine discharge in early spring. We therefore suggest that winter and spring subglacial upwelling is not unique to Billefjorden, but likely occurs at all polythermal or warm-based marine terminating glaciers.~~

The amount of discharge and upwelling was estimated using hydrographic data. In our study, three water masses were distinguished; i) subglacial outflow (SGO) with low salinity (0 PSU) relatively high temperatures (>0 °C) and high silicate concentrations (Cape et al., 2019), (ii) deep local Arctic water (DLAW) entrained from approx. 20 m with low temperatures (-1.7 °C) high salinities (34.6 PSU) and high nutrient concentrations (Skogseth et al., 2020), and iii) surface local Arctic water (SLAW) with the same temperature and salinity signature as the DLAW, but depleted in nutrients (Skogseth et al., 2020). Nutrients were depleted in the UIW, but not at 15 m depth, showing that the nutricline had to be shallower than 15 m. Hence, submarine discharge depth at a glacier terminus depth of 20 m would be sufficient to cause upwelling of nutrient rich DLAW to the surface. In fact, oOur mixing calculations (Equations 1-6) estimate that 32 % of the SG water 1 m under the sea ice was derived by SGO, which pulled 1.6 times ~~more as much~~ (53 % DLAW : 32 % SGO = ratio of 1.6) DLAW with it during upwelling. Fransson et al. (2020) found that 30-60 % of glacier derived meltwater was incorporated in the bottom sea ice at the glacier front of Tempelfjorden, again indicating that early spring submarine discharge and the resulting formation of sea ice with low porosity~~this~~ is a widespread process at marine terminating glacier fronts.

553 **4.3 Importance of subglacial-submarine discharge and upwelling under sea ice**

554 To our knowledge, our study provides currently the only available estimate of subglacial upwelling in early spring. Our study suggests that subglacial upwelling in spring resultscauses in Billefjorden in-a small volume transport of only about >1.1 m³ m⁻² month⁻¹ (approx. 2 m³ s⁻¹). This estimate is based on the flux of nutrient rich bottom water needed to maintain the measured primary production assuming steady state conditions and is therefore a rough, but conservative estimate. The most comparable

558 estimate on the magnitude of the upwelling is available at Kronebreen for summer. This Svalbard tidewater glacier is of similar
 559 size and had one to two orders of magnitude higher upwelling rates compared to our study ($31\text{--}127\text{ m}^3\text{ s}^{-1}$, Halbach et al.,
 560 2019). Due to their size, summer subglacial upwelling in Greenland is two to four times higher than at Kronebreen ($250\text{--}500$
 561 $\text{m}^3\text{ s}^{-1}$, Carroll et al., 2016). In our study about 1.6 times as much bottom water from about 20 m (DLAW) as subglacial outflow
 562 water (SOW) reached the surface at SG (Entrainment factor of 1.6 – see above). The entrainment factor is mostly dependent
 563 on the depth of the glacier front (Carroll et al., 2016). In fact, the glacier terminus at SG was shallower (approx. 20 m) than
 564 any other studied tidewater glacier on Svalbard (70 m depth at Kronebreen, Halbach et al., 2019) or Greenland ($> 100\text{ m}$,
 565 Hopwood et al., 2020), explaining ~~the higher summer entrainment factors estimated in Kongsfjorden (3, Halbach et~~
 566 ~~al., 2019) and Greenland (6 to 10, Hopwood et al., 2020) are not surprising.~~ Glacier terminus depth appears to be the main
 567 control of entrainment rates, likely independent of the time of the year. However, turbulent mixing may cause increased
 568 entrainment during times of very high subglacial discharge rates. Kronebreen is the most comparable tidewater glacier to our
 569 study area in terms of glacier terminus depth and entrainment rate. Although the estimated entrainment factor was low at
 570 Kronebreen (3), it substantially increased summer primary production in Kongsfjorden (Halbach et al., 2019). ~~In spite of~~
 571 ~~the shallow depth, and the low discharge and entrainment rate of our study, subglacial upwelling appears to be~~ was the main
 572 ~~mechanism to replenish bottom water with high nutrient concentrations to the surface and can~~ substantially increased spring
 573 ~~primary production due to;~~ (i) submarine outflow below (approx. 20 m) the nutricline ($<15\text{ m}$), (ii) the absence of any other
 574 ~~terrestrials inputs, (iii) Atlantic water blocked by a shallow sill (Skogseth et al., 2020), (iv) very weak tidal currents (Kowalik~~
 575 ~~et al., 2015), (iv) wind mixing blocked by sea ice in Billefjorden, and (v) undiluted subglacial meltwater having lower nutrient~~
 576 ~~concentrations than the DLAW. Compared to the massive subglacial plumes of summer systems ($250\text{--}500\text{ m}^3\text{ s}^{-1}$, Hopwood~~
 577 ~~et al., 2020), subglacial upwelling in spring is a small volume transport with only about $>1.1\text{ m}^3\text{ m}^{-2}\text{ month}^{-1}$ upwelling needed~~
 578 ~~to sustain measured surface primary production. This careful estimate translates to a freshwater input for Billefjorden of at~~
 579 ~~least $1.76 \times 10^5\text{ m}^3\text{ day}^{-1}$, which is one order of magnitude lower than summer values at Kronebreen ($2.7 \times 10^6\text{ m}^3\text{ day}^{-1}$,~~
 580 ~~Halbach et al., 2019), a Svalbard tidewater glacier of similar size. In addition, less bottom water was entrained with subglacial~~
 581 ~~outflow water (lower entrainment factor) compared to other subglacial upwelling studies (e.g. Hopwood et al., 2020). In our~~
 582 ~~study, each volume of SGO water pulled about the same volume of DLAW with it to the surface (Entrainment factor of 1.6 –~~
 583 ~~see above). This value is low compared to other entrainment factor estimates ranging mostly between 6 and 10 (Hopwood et~~
 584 ~~al., 2020). The entrainment factor is mostly dependent on the depth of the glacier front (Hopwood et al., 2020), which can~~
 585 ~~explain the low rate at Nordenskiöldbreen in Billefjorden, with an estimated depth of 20 m at the terminus (based on CTD east~~
 586 ~~at terminus in April 2018, data not shown). Kronebreen with a glacier terminus depth of about 70 m and an entrainment factor~~
 587 ~~of 3 is the most comparable tidewater glacier to Nordenskiöldbreen, where these fluxes were estimated. Although entrainment~~
 588 ~~rate was low, it substantially increased summer primary production in Kongsfjorden (Halbach et al., 2019). In spite of the low~~
 589 ~~discharge and entrainment rate of our study, subglacial upwelling appears to be the main mechanism to replenish bottom water~~
 590 ~~with high nutrient concentrations to the surface and can substantially increase spring primary production due to;~~ i) the absence

~~of any other terrestrials inputs, ii) Atlantic water blocked by a shallow sill (Skogseth et al., 2020), iii) very weak tidal currents (Kowalik et al., 2015), and iv) wind mixing blocked by sea ice in Billefjorden.~~

4.4 Importance for under-ice phytoplankton

Our main finding was that i) higher irradiance, ii) a stratified surface layer, and iii) increased nutrient supply via subglacial upwelling allowed increased phytoplankton primary production at SG. ~~Surprisingly,~~ The ice edge station (IE) was light and nutrient limited and supported a lower phytoplankton primary production.

4.4.1 Increased light

Despite the ~~substantial~~ subglacial upwelling, the negative effect of light limitation with the massive sediment plumes in summer (Pavlov et al., 2019) were not observed in early spring. We did measure a small turbidity peak under the SG sea ice, but the values were comparable to open fjord systems in summer (Meslard et al., 2018, Pavlov et al., 2019), where light is ~~not considered limiting sufficient for photosynthesis~~. Under-ice phytoplankton blooms are typically limited by light, which is attenuated and reflected by the snow and sea ice cover (Fortier et al., 2002, Mundy et al., 2009, Ardyna et al., 2020). Some blooms have been observed, mostly under snow-free sea ice, such as after snow melt (Fortier et al., 2002), under melt ponds (Arrigo et al., 2012, Arrigo et al., 2014), after rain events (Fortier et al., 2002), or at the ice edge related to ~~ice-edgewind-induced driven Ekman~~ upwelling (Mundy et al., 2009). In our study however, light levels available for phytoplankton growth were low compared to other under-ice phytoplankton bloom studies (Mundy et al., 2009, Arrigo et al., 2012), but higher at SG than at IE. This can be explained through the combined effects of sea ice and snow properties at SG. Light attenuation in low salinity sea ice is typically lower due to a lower brine volume (Arst and Sipelgas, 2004). Also, lower sea ice algae biomass and thinner snow cover due to snow removal with katabatic winds (e.g. Braaten 1997; Laska et al., 2012) leads to less light attenuation and a lower albedo. Our estimates showed that about twice as much light reached the water at SG compared to the IE, in spite of the thicker sea ice cover and the estimated light levels of 5 and 9 $\mu\text{E m}^{-2} \text{s}^{-1}$ were above the minimum irradiance (1 $\mu\text{E m}^{-2} \text{s}^{-1}$) required for primary production (Mock & Gradinger, 1999). Hence, the increased light under the brackish sea ice at SG could be one factor explaining the under-ice phytoplankton bloom observed.

4.4.2 Stratified surface layer

The strong stratification at SG is another factor; allowing phytoplankton to stay close to the surface, where light is available, allowing a bloom to form. In fact, Lowry et al. (2017) found that convective mixing by brine expulsion in refreezing leads can inhibit phytoplankton blooms even in areas with sufficient under-ice light and nutrients. At the same time, they found moderate phytoplankton blooms under snow covered sea ice (1–3 mg Chl m^{-3}) sustained by a more stratified surface layer, which was, however, still an order of magnitude lower than the SG values. Our finding of a higher vertical flux at IE compared to SG shows that stronger stratification may indeed be a contributing factor for the higher phytoplankton biomass at SG due to lower

loss rate. However, our reciprocal transplant experiment clearly showed, that location alone (light, stratification) could not explain the increased primary production, but that the water properties at SG had a fertilising effect on algal growth, most probable because of higher nutrient levels, which were limiting at IE.

4.4.3 Upwelling and meltwater influx of nutrients

Algal growth at IE was co-limited by lower irradiance as well as nutrient concentrations. Dissolved inorganic nitrogen (DIN) to phosphate ratios (N:P) at the IE were mostly below Redfield ratios (16:1), especially in sea ice with DIN concentrations below $1 \mu\text{mol L}^{-1}$, indicating potential nitrogen limitations (Ptacnik et al., 2010), while the N:P ratio at SG was balanced and close to Redfield. Silicate concentrations below $2 \mu\text{mol L}^{-1}$ are typically considered limiting for diatom growth (Egge & Aksnes, 1992) and this threshold had been reached at UIW and sea ice (concentration estimate in brine volume) at IE, but not at SG. This indicates that nitrate supplied by deep-bottom water upwelling and silicate by combined upwelling and additions from the glacial run off had a fertilising effect on the SG water-. High silicate values have also been observed at glacier fronts in other areas such as the Greenland fjords (Azetsu-Scott and Syvitski, 1997) and Tempelfjorden (Fransson et al., 2015:2020). Iron has not been measured, but is an essential micronutrient, often enriched in subglacial meltwater (Bhatia et al., 2013, Hopwood et al., 2020). However, iron limitation ~~is unlikely in these systems~~untypically does not occur in coastal Arctic systems (HopwoodKrisch et al., 2020). Besides the subglacial upwelling, nutrient concentrations ~~may simply be~~could be higher due to ~~due to less~~lower physical forcing and time needed for vertical mixing at the shallower water depth at SG compared to IE, facilitating vertical mixing down to the bottom. However, NG was slightly shallower than SG and algal growth was still limited by nutrients. Besides, ~~neither~~ silicate ~~nor~~and nitrate ~~followed a conservative mixing pattern~~showed negative correlations with salinity, when including SG samples. In fact, these nutrients only ~~mixed conservatively~~correlated positively with salinity at IE and NG, ~~but showed while at SG, the negative correlations or~~ non-conservative mixing ~~at SG, which is a clear evidence~~are indicative for subglacial upwelling (mainly N and Si) and/or meltwater input (for Si) (Hopwood et al., 2020). Biological nutrient uptake did not play a significant role, due to relatively low bacterial and primary production. The subglacial outflow water itself was poor in nitrate, but high in silicate due to the interaction with the bedrock and long residence time below the glacier (Wadham et al., 2001), which was also found in the Tempelfjorden (Fransson et al., 2015; 2020). Nordenskiöldbreen has a mix of metamorphic bedrock including silicon rich gneiss, amphibolite, and quartzite, but also carbonate rich marble (Strzelecki, 2011), which can partly contribute to the high silicate levels observed. The role of bedrock derived minerals and particles for composition of sea ice chemistry have been described in the neighbouring fjord (Tempelfjorden) in detail by Fransson et al. (2020). Silicate concentrations ~~The values~~ in subglacial outflow water were lower ($<1.5 - 2 \mu\text{mol L}^{-1}$) compared to estimates in Greenland (~~Hawkins~~Meire et al., 2016a, Hawkings et al., 2017, Hatton et al., 2019), indicating that direct fertilisation in early spring may be even more important in other tidewater glacier influenced fjords. Another potential source may be higher silicate concentrations in the sediments at SG (Hawkings et al., 2017). However-, bottom water values were similar between SG and IE, showing a limited role of higher silicate inputs from sediment-

654 Besides, iron may be supplied via subglacial outflow (Bhatia et al., 2013, Hopwood et al., 2020), but it is most likely not
655 limiting in coastal systems (Hopwood et al., 2020), presumably due to silicate-poor subglacial bedrock.
656 Another nitrogen source may be ammonium, which ~~has been related to~~ was introduced via subglacial upwelling in
657 Kongsfjorden (Halbach et al., 2019). Ammonium regeneration and subsequent nitrification (Christman et al., 2011) ~~under the~~
658 ~~sea ice,~~ may explain the exceptionally high nitrate concentration of the UIW at SG-, ~~which can be part of the~~
659 ~~explanation partially explain for the high N:P ratios.~~ In fact, bacterial activity was higher at SG potentially allowing higher
660 ammonium recycling. ~~Another explanation for the high N:P ratios and low phosphate concentrations can be related to~~ could be
661 ~~phosphate scavenging by iron,~~ as discussed by Cantoni et al. (2020). ~~Nitrate can be supplied through the subglacial meltwater~~
662 ~~itself (Wynn et al., 2007), however we did not find high nitrate concentrations in the undiluted subglacial outflow water in our~~
663 ~~study.~~ Atmospheric inputs of N have been shown in the Baltic Sea, but thinner sea ice and warm periods with increased sea
664 ice permeability were needed for the N to reach the brine pockets or water column (Granskog et al., 2003). Our NO_x profiles
665 show some evidence of atmospheric N deposition, but only at NG and SG, which may be related to precipitation or surface
666 flooding. For under-ice phytoplankton, these atmospheric N inputs play no role, but may have benefitted the high
667 *Leptocylindrus* algae biomass layer in the upper ice parts of SG. Overall, the clearest evidence of nutrient limitations and
668 fertilisation by ~~subglacial-submarine discharge and~~ upwelling was demonstrated with the reciprocal transplant experiment,
669 which showed an approx. 30 % increase in primary production ~~related to~~ of algae communities incubated in SG water. Overall,
670 primary production at SG was an order of magnitude higher than at IE. This indicates that both fertilisation by ~~subglacial~~
671 ~~submarine discharge and~~ upwelling and increased light ~~and stratification~~ play a role in increasing phytoplankton primary
672 production.

673 4.4.4 Increased phytoplankton primary production

674 The integrated primary production to 25 m at SG was 42.6 mg C m⁻² d⁻¹ which is low compared to other marine terminating
675 glacier influenced fjord systems in summer with integrated NPP of 480 ~~±403~~ mg C m⁻² d⁻¹ (Hopwood et al., 2020), ~~including~~
676 ~~studies in Kongsfjorden on Svalbard with 250 -900 mg C m⁻² d⁻¹ (Van de Poll et al. 2018). Also A studies in the~~
677 ~~same conducted during a similar time window as ours month (April time (1 May))~~ observed higher primary production rates in
678 a marine-terminating glacier influenced fjord system, ~~such as in~~ Kongsfjorden (405 ~~1520-1850~~ mg C m⁻² d⁻¹, ~~Hopwood~~ Hodal
679 et al., 2012). However, none of these systems was sea ice covered during the studies and therefore not limited by light
680 compared to our study. Under sea ice, phytoplankton communities have typically much lower NPP rates of 20–310 mg C m⁻²
681 d⁻¹ with only about 10 % or less light transmission reaching the water column (Mundy et al., 2009). These values are more
682 comparable to the SG values, despite the lower ~~estimated~~ light transmission (3 %). In the central Arctic, higher under-ice NPP
683 has been observed, but always related to high light transmission due to the absence of ice, or under melt ponds with light
684 transmissions up to 59 % (Arrigo et al., 2012). However, in the sea ice area north of Svalbard, Assmy et al. (2017) found
685 substantial spring PP below relatively thick sea ice ~~caused by~~ of refrozen leads. This was also confirmed by a large CO₂ decrease
686 due to primary production under the sea ice (Fransson et al., 2017). Phytoplankton production under snow covered Arctic sea

ice is often considered negligible compared to sea ice algae or summer production. This can be shown in low biomass, mostly consisting of settling sea ice algae (Leu et al., 2015), or very low NPP rates (e.g. Pabi et al., 2008). The same has been observed under Baltic sea ice with similar low light levels and primary production between 0.1–5 mg C m⁻² d⁻¹ under snow covered sea ice and about 30 mg C m⁻² d⁻¹ under snow-free sea ice (Haecky & Andersson, 1999). These values are comparable to the IE without subglacial meltwater influence, but an order of magnitude lower than the SG production. Moderate blooms of 1–3 mg Chl m⁻³ have been described under snow covered sea ice with equal (3 %) light transmission (Lowry et al., 2017). Lowry et al. (2017) argues that a stratified water column and sufficient nutrients allow moderate blooms even under these low light conditions. In particular, diatoms, the most common taxa of under-ice phytoplankton blooms (von Quillfeldt, 2000, this study) are known to be well adapted to low light conditions (Furnas, 1990). Our study found Chl values up to an order of magnitude higher than Lowry et al. (2017), showing that under-ice phytoplankton blooms are indeed important under snow covered sea ice and can be facilitated by subglacial-submarine discharge and upwelling.

Our study is the first to show that the combination of several factors (stratified water column, increased light and supply of fresh nutrients via tidewater glacier driven processes) can support a rather productive under-ice phytoplankton community, exceeding biomass and production of under-ice phytoplankton in systems with comparable light levels. Besides the increased and extended primary production fuelled by tidewater glacier, the active and abundant phytoplankton taxa in surface water with consistently replenished nutrients, ~~are~~may be a viable seed community for summer phytoplankton blooms, once the sea ice disappears and light levels increase (Hegseth et al., 2019). The significantly different community at SG may also contribute to a more diverse seed community available to the entire fjord, compared to fjords without early spring subglacial upwelling~~discharge~~.

4.5 Impact on sea ice algae

4.5.1 Impact on biomass and primary production

While phytoplankton biomass and production were clearly enhanced at SG, exceeding levels of other snow-covered under-ice systems, sea ice algal biomass and activity had been differently affected. Our third hypothesis suggested lower sea ice algae biomass and production at SG due to the lower brine volume fractions. In agreement with our hypothesis, algal biomass was indeed an order of magnitude lower compared to the IE and NG. However, ~~their~~primary production was two times higher, showing more efficient photosynthesis.

Compared to most other sea ice studies conducted at the same period of the year, typically representing the mid-bloom phase with 10–20 mg Chl m⁻² (Leu et al., 2015), Chl biomass was very low at all stations of our study (<0.32 mg Chl m⁻²). Only Greenland fjords (0.~~5~~1-3.3 mg Chl m⁻²) or pre- and post-bloom systems had comparably low biomass (Mikkelsen et al., 2008, Leu et al., 2015). The significantly different communities with a-high-number of cryptophyte flagellates, a high proportion of phaeophytin (14–68 % in the bottom 3 cm), and ~~the a~~high contribution of sea ice algae in the water column indicate that we sampled indeed a post-bloom situation. Considering the low air, sea ice and water temperatures and the absence of a fresh

719 UIW layer at the IE, the bloom was most likely not terminated by bottom ice erosion but limited by nutrients. In fact, SG
 720 bottom ice was ~~limited by~~deficient in phosphate ($0.27 \mu\text{mol (L brine)}^{-1}$), while the IE was ~~limited by~~deficient in silicate (1
 721 $\mu\text{mol (L brine)}^{-1}$) and nitrogen ($\text{N:P} = 1 \text{ mol N mol P}^{-1}$). This finding fits to earlier studies where phosphate limitations had
 722 been described as limiting for brackish sea ice algae at concentrations below $0.27 \mu\text{mol L}^{-1}$ (Haecky and Andersson, 1999),
 723 while N and Si limitations are typical for Arctic sea ice algae (Gradinger, 2009). The low concentrations of phosphate in the
 724 subglacial meltwater would partly explain the low concentration in SG sea ice. In addition, most studies summarized by Leu
 725 et al. (2015) were done 10 years or more prior to our measurements. In fact, the Greenland study by Mikkelsen et al. (2008)
 726 with comparable sea ice algae biomass had the thinnest sea ice cover of 0.5 m sampled in the warmest year (2006). During our
 727 study, the weather station in Longyearbyen measured a mean temperature of -3.9°C in April 2019, which was -8.3°C above
 728 average and the second warmest average April temperature recorded after April 2006 (0.1°C), indicating that a warmer climate
 729 may explain the earlier bloom termination (yr.no).
 730 Similar to algal biomass, primary production (approx. $0.01 \text{ mg C m}^{-2} \text{ d}^{-1}$ at SG and $0.005 \text{ mg C m}^{-2} \text{ d}^{-1}$ at IE, assuming 10 cm
 731 productive bottom layer) was considerably lower than in most studies of Arctic sea ice ($0.8\text{--}55 \text{ mg C m}^{-2} \text{ d}^{-1}$ in the Barents
 732 Sea) mentioned by Leu et al.(2015). Only algal aggregates (Assmy et al., 2013) and Baltic sea ice (Haecky & Andersson,
 733 1999) measured similarly low production rates indicating that the senescence of the bloom (aggregates) and brine volume
 734 fraction (Baltic Sea) were factors contributing to low primary production in sea ice.

735 **4.5.2 Stressors in brackish sea ice**

736 In addition to the post bloom status of the bloom, the lower biomass at SG can be partly explained by the lower brine salinity.
 737 Permeability of sea ice is typically related to salinity and temperature, which determine the brine volume. With a brine volume
 738 fraction below 5 %, or temperature below -5°C and salinity below 5 PSU, sea ice is considered impermeable (Golden et al.,
 739 1998). At SG, temperatures were higher, but a brine volume fraction above 5 % was only found in bottom ice sections (7–9
 740 %), indicating that the brine channels are weakly connected and algae had limited inhabitable place and nutrient supply
 741 (Granskog et al., 2003), especially in the upper layers of the sea ice. In more saline systems, such as the Chuckchi or Beaufort
 742 Sea a high flux of seawater through the ice ($0.4\text{--}19 \text{ m}^3 \text{ seawater m}^{-2} \text{ sea ice}$) has been discussed as crucial to allow continuous
 743 primary production and accumulation of biomass (Gradinger, 2009). In impermeable ice, this flux is eliminated. However, the
 744 algal biomass at SG was very low, even compared to other brackish sea ice system, such as the Baltic Sea with similar or lower
 745 brine volume fractions and comparable light levels (Granskog et al., 2003: $3\text{--}6 \text{ mg Chl m}^{-3}$; Haecky & Andersson, 1999: 1.2
 746 mg Chl m^{-2}), indicating that other stressors played a role at SG. Grazing is assumed to be a minor control on algae production
 747 and biomass in Arctic sea ice (Gradinger, 2002). However, grazing by heterotrophic flagellates on small primary producers
 748 has been described as important in the Baltic Sea, indicating that it might plays a role at SG as well (Haecky & Andersson,
 749 1999). SG sea ice communities were indeed dominated by small flagellate algae (microscopy based) and a high proportion of
 750 potential grazers (18S rRNA data). Other stressors, such as phosphate limitation, viral lysis, or osmotic stress related to episodic
 751 outbursts of subglacial meltwater are likely additional factors explaining the low biomass.

752 DIC has also been described as potentially limiting for sea ice primary production, especially towards the end of the bloom
753 (Haecky & Andersson, 1999) and may be supplied with the carbonate rich subglacial outflow (Fransson et al., 2020). Higher
754 mortality due to factors mentioned above, together with the higher measured bacterial activity, allowing recycling of nutrients
755 may be another factor explaining higher production with lower Chl biomass. Last, nutrients may have been replenished recently
756 via advective processes when the brine volume fraction was higher.

757 At SG₂, another layer of potentially high activity has been found in the upper sea ice. In this layer, depleted nutrient
758 concentrations correspond with high *Leptocylindrus minimus* abundances indicating that these algae were actively taking up
759 the nutrients, despite the impermeable sea ice. NO_x concentrations increased towards the surface and bottom indicating inputs
760 from surface flooding above (Granskog et al., 2003) and seawater below. Silicate and phosphate were only supplied from the
761 seawater below. The observed brine volume fractions below 5 % would not allow inputs of these nutrients, but episodes with
762 higher temperatures and thereby higher brine volume fractions may be sufficient to supply the needed nutrients to this
763 distinctive layer.

764 Overall, sea ice influenced by subglacial outflow was very similar to other brackish sea ice such as in the Baltic Sea in regard
765 to structure, biomass and production (Haecky & Andersson, 1999, Granskog et al., 2005). Compared to Arctic sea ice the
766 effect was negative on sea ice algae biomass due to low brine volume fractions, phosphate limitation and potentially higher
767 mortality via grazing and possibly higher osmotic stress.

768 5 Outlook

769 Our study showed that even a shallow marine-terminating glacier can lead to increased under-ice phytoplankton production
770 by locally enhanced light levels, stronger stratification and nutrient supply by subglacial-submarine discharge and upwelling,
771 which are all factors expected to change due to climate change. While most of our evidence is circumstantial, the number of
772 different evidence leading to the same conclusion makes our findings rather robust. We propose that our findings are applicable
773 to other tidewater glaciers with a polythermal or warm base, as is common on Svalbard, but also on Greenland (Hagen et al.,
774 1993; Irvine-Fynn et al., 2011). In the shorter term, a longer melt season and presumably increased submarine discharge may
775 lead to increased subglacial upwelling in winter and spring. However, on longer time scales-, ~~With a changing climate,~~
776 ~~tidewater~~ glaciers will retreat and transform towards land terminating glaciers (Błaszczyk et al., 2009), which, ~~In winter and~~
777 ~~spring, this~~ would result in the lack of subglacial upwellingsubmarine discharge and systems more similar to the IE with less
778 nutrients and light available for phytoplankton. The local effect would reduce primary production, biomass and bacterial
779 production in the water column, but higher biomass of sea ice algae with the known Arctic taxa of pennate diatoms. The
780 pelagic/sympagic benthic coupling would be stronger supporting the benthic food web. ~~In addition, the lack of upwelling will~~
781 ~~have consequences for summer production, which is dependent on algae seeds for the development of phytoplankton blooms~~
782 ~~(Hegseth et al., 2019). In absence of subglacial upwelling and wind mixing blocked by sea ice or slow tidal currents, the seed~~
783 ~~material from the deeper sediments would not reach the water column, leading to a reduced and delayed phytoplankton summer~~
784 ~~bloom.~~ Winter and spring subglacial upwelling-submarine discharge is most likely present at all polythermal or warm-based

marine-terminating glaciers, which includes glacier termina with much deeper fronts, ~~and~~ much higher entrainment rates of bottom water, and higher silicate concentrations in the glacial meltwater (Hopwood et al., 2020). Thus, the effect of early spring ~~subglacial upwelling~~ submarine discharge is likely more pronounced in other fjords. Additional effects of climate change include increased precipitation in the Arctic, which would reduce light levels below the sea ice. However, also land-terminating glaciers would allow snow removal by katabatic wind as discussed for Nordenskiöldbreen.

Another impact of climate change will be the reduction and earlier break-up of sea ice and Atlantification of fjords, leading to increased light, and wind mixing. In the ice free Kongsfjorden, higher primary production rates have been measured in the same month, indicating that the lack of sea ice may lead to increased overall primary production (Iversen & Seuthe, 2010). However, Kongsfjorden is still influenced by subglacial upwelling, supplying nutrients for the bloom (Halbach et al., 2017). In systems not affected by subglacial upwelling the additional light will most likely not lead to substantially higher primary production as indicated by lower measured rates in these type of fjords (Hopwood et al., 2020). Since the entrainment in our study occurs at only approximately 20 m depth, upwelling under sea ice-free conditions would have much less effect, since wind induced vertical mixing plays a more important role. Direct silicate fertilisation would also have less effect in an ice-free fjord since the fjord phytoplankton biomass is likely more nitrate than silicate limited, due to the later stage of the spring bloom (Hegseth et al., 2019). In summary, we suggest that subglacial upwelling in early spring is important for phytoplankton blooms, but only in a sea-ice covered fjord. The future of the spring phytoplankton blooms depends on what happens first, disappearance of sea ice, or retreat of the glacier to land.

6 Acknowledgements

The field was funded by the individual Arctic field grants of the Svalbard Science forum for TV, UD, CD, and EH (project numbers: 282622 (TV, UD, CD), 282600 (TV), 296538 (EH), 281806 (UD)). Additional, funding for lab work and analyses was obtained by the ArcticSIZE - A research group on the productive Marginal Ice Zone at UiT (grant no. 01vm/h15). JE was also supported by the the Ministry of Education, Youth and Sports of the Czech Republic ECOPOLARIS, project No. CZ.02.1.01/0.0/0.0/16_013/0001708 and the Institute of Botany CAS (grant no. RVO 67985939). The publication charges for this article have been partly funded by a grant from the publication fund of UiT The Arctic University of Norway.

We also wish to thank Jan Pechar, Jiří Štojd, and Marie Šabacká for field assistance; and Janne Søreide, Maja Hatlebekk, Christian Zoelly, Marek Brož, Stuart Thomson, and Tore Haukås for field work preparation help. We are also acknowledged to Melissa Brandner, Paul Dubourg, and Claire Mourgues for the help in the lab and Owen Wangensteen for the help with bioinformatics analyses. We are thankful for the meteorological data of Petuniabukta supplied by Kamil Laska.

813 **7 Authors contributions**

814 TRV designed the experiments, formulated the hypotheses and developed the sampling design with contributions of CD and
815 UD, and RG. Fieldwork was conducted by TRV, UD, CD, EH, and JE with support by RG and EP for preparations. Lab
816 analyses were done by TRV, UD, EP, CD, MC and EH. Computational analyses were performed by TRV. The manuscript has
817 been prepared by TRV with contributions of all co-authors.

818 **8 Data availability**

819 Environmental data have been archived at Dataverse under the doi number <https://doi.org/10.18710/MTPR9E>. 18S and 16S
820 rRNA sequences have been archived at the European Nucleotide archive under the project accession number PRJEB40294.
821 The R and unix code for the statistical and bioinformatics analyses are available from the corresponding author upon request.
822 More detailed reports of the fieldwork are available in the Research in Svalbard database under the RiS-ID 10889.

823 **9 Competing interests**

824 The authors declare that they have no conflict of interest.

825 **References**

826 Ambrožová, K., and Láska, K.: Air temperature variability in the vertical profile over the coastal area of Petuniabukta, central
827 Spitsbergen, Polish Polar Research, 41-60, 2017.

828 [Amundson, J. M., and Carroll, D.: Effect of topography on subglacial discharge and submarine melting during tidewater glacier](#)
829 [retreat, Journal of Geophysical Research: Earth Surface, 123\(1\), 66-79, 2018.](#)

830 Ardyna, M., Mundy, C. J., Mills, M. M., Oziel, L., Grondin, P. L., Lacour, L., Verin, G., Van Dijken, G., Ras, J., Alou-Font,
831 E., Babin, M., Gosselin, M., Tremblay, J. É., Raimbault, P., Assmy, P., Nicolaus, M., Claustre, H. and Arrigo, K.R.:
832 Environmental drivers of under-ice phytoplankton bloom dynamics in the Arctic Ocean, Elem Sci Anth, 8(1), 30, DOI:
833 <http://doi.org/10.1525/elementa.430>, 2020.

834 Arrigo, K. R., Perovich, D. K., Pickart, R. S., Brown, Z. W., vanDijken, G. L., Lowry, K. E., Mills, M. M., Palmer, M. A.,
835 Balch, W. M., Bahr, F., Bates, N. R., Benitez-Nelson, C., Bowler, B., Brownlee, E., Ehn, J. K., Frey, K. E., Garley, R.,
836 Laney, S.R., Lubelczyk, L., Mathis, J., Matsuoka, A., Mitchell, G. B., Moore, G. W. K., Ortega-Retuerta, E., Pal, S.,
837 Polashenski, C.M., Reynolds, R. A., Schieber, B., Sosik, H. M., Stephens, M., P., and Swift, J. H.: Massive phytoplankton
838 blooms under Arctic sea ice, Science, 336, 1408, <https://org/10.1126/science.1215065>, 2012.

839 Arrigo, K. R., Arrigo, K. R., Perovich, D. K., Pickart, R. S., Brown, Z. W., van Dijken, G. L., Lowry, K. E., Mills, M. M.,
840 Palmer, M. A., Balch, W. M., Bates, N. R., Benitez-Nelson, C. R., Brownlee, E., Frey, K. E., Laney, S. R., Mathis, J., Matsuoka,

841 A., Mitchell, B. G., Moore, G. W. K., Reynolds, R. A., Sosik, H. A., Swift, J. H.: Phytoplankton blooms beneath the sea ice in
842 the Chukchi Sea, Deep Sea Res. Part II Top. Stud. Oceanogr., 105, 1-16, <https://org/10.1016/j.dsr2.2014.03.018>, 2014.

843 Arst, H., and Sipelgas, L.: In situ and satellite investigations of optical properties of the ice cover in the Baltic Sea region, in:
844 Proceedings of the Estonian Academy of Sciences, Biology and Ecology, edited by: Aben, H., and Kurnitski, V., Estonian
845 Academy of Sciences, Tallinn, 25-36, 2004.

846 Assmy, P., Ehn, J. K., Fernández-Méndez, M., Hop, H., Katlein, C., Sundfjord, A., Bluhm, K., Daaase, M., Engel, A., Fransson,
847 A., Granskog, M. A., Hudson, S. R., Kristiansen, S., Nicolaus, M., Peeken, I., Renner, A. H. H., Spreen, G., Tatarek, A., and
848 Wiktor, J.: Floating ice-algal aggregates below melting Arctic sea ice, PLoS ONE, 8(10), e76599,
849 <https://org/10.1371/journal.pone.0076599>, 2013.

850 Assmy, P., M. Fernández-Méndez, P. Duarte, A. Meyer, A. Randelhoff, C. J. Mundy, L. M. Olsen, H. M. Kauko, A. Bailey, and
851 Chierici, M.: Leads in Arctic pack ice enable early phytoplankton blooms below snow-covered sea ice, Scientific reports, 7,
852 40850, 2017.

853 Atienza, S., Guardiola, M., Præbel, K., Antich, A., Turon, X., and Wangenstein, O. S.: DNA Metabarcoding of Deep-Sea
854 Sediment Communities Using COI: Community Assessment, Spatio-Temporal Patterns and Comparison with 18S rDNA,
855 Diversity, 12(4), 123, <https://org/10.3390/d12040123>, 2020.

856 Azetsu-Scott, K., and Syvitski, J. P. M.: Influence of melting icebergs on distribution, characteristics and transport of marine
857 particles in an East Greenland fjord, Journal of Geophysical Research 104 (C3), 5321–5328, 1999.

858 Bhatia, M. P., Kujawinski, E. B., Das, S. B., Breier, C. F., Henderson, P. B., and Charette, M. A.: Greenland meltwater as a
859 significant and potentially bioavailable source of iron to the ocean, Nat Geosci, 6(4), 274-278, <https://org/10.1038/ngeo1746>,
860 2013.

861 Błaszczyk, M., Jania, J. A., and Hagen, J. O.: Tidewater glaciers of Svalbard: Recent changes and estimates of calving fluxes,
862 Pol Polar Res, 2, 85-142, 2009.

863 Boyer, F., Mercier, C., Bonin, A., Le Bras, Y., Taberlet, P., and Coissac, E.: obitools: A unix-inspired software package for
864 DNA metabarcoding, Mol Ecol Resour, 16(1), 176-182, <https://org/10.1111/1755-0998.12428>, 2016.

865 Braaten, D. A.: A detailed assessment of snow accumulation in katabatic wind areas on the Ross Ice Shelf, Antarctica, J
866 Geophys Res Atmos, 102(D25), 30047-30058, <https://org/10.1029/97JD02337>, 1997.

867 Cantoni, C., Hopwood, M. J., Clarke, J. S., Chiggiato, J., Achterberg, E. P., and Cozzi, S.: Glacial drivers of marine
868 biogeochemistry indicate a future shift to more corrosive conditions in an Arctic fjord, Journal of Geophysical Research:
869 Biogeosciences, e2020JG005633, <https://doi.org/https://doi.org/10.1029/2020JG005633>, 2020.

870 Carroll, D., Sutherland, D. A., Hudson, B., Moon, T., Catania, G. A., Shroyer, E. L., Nash, J. D., Bartholomaeus, T. C., Felikson,
871 D., Stearns, L. A., Noël, B. P. Y., and van den Broeke, M. R.: The impact of glacier geometry on meltwater plume structure
872 and submarine melt in Greenland fjords, Geophys. Res. Lett., 43, 9739–9748, <https://doi.org/10.1002/2016GL070170>, 2016.

873 Chandler, D. M., Wadham, J. L., Lis, G. P., Cowton, T., Sole, A., Bartholomew, I., Telling, J., Nienow, P., Bagshaw, E.B.,
874 Mair, D., Vinen, S., and Hubbard A.: Evolution of the subglacial drainage system beneath the Greenland Ice Sheet revealed
875 by tracers, *Nat Geosci*, 6(3), 195-198, <https://org/10.1038/ngeo1737>, 2013.

876 Christman, G. D., Cottrell, M. T., Popp, B. N., Gier, E., and Kirchman, D. L.: Abundance, diversity, and activity of ammonia-
877 oxidizing prokaryotes in the coastal Arctic Ocean in summer and winter, *Appl. Environ. Microbiol.*, 77(6), 2026-2034,
878 <https://org/10.1128/AEM.01907-10>, 2011

879 Cloern, J. E., Grenz, C., and Videgar-Lucas, L.: An empirical model of the phytoplankton chlorophyll: carbon ratio-the
880 conversion factor between productivity and growth rate, *Limnol. Oceanogr.*, 40(7), 1313-1321,
881 <https://org/10.4319/lo.1995.40.7.1313>, 1995.

882 Cox, G. F., and Weeks, W. F.: Equations for determining the gas and brine volumes in sea-ice samples, *J Glaciol*, 29(102),
883 306-316, <https://org/10.3189/S0022143000008364>, 1983.

884 De Kluijver, A., Soetaert, K., Czerny, J., Schulz, K. G., Boxhammer, T., Riebesell, U., and Middelburg, J. J.: A ¹³C labelling
885 study on carbon fluxes in Arctic plankton communities under elevated CO₂ levels, *Biogeosciences*, 10(3), 1425-1440, 2013.

886 Dickson, A. G., Sabine, C. L., and Christian, J. R.: Guide to best practices for ocean CO₂ measurements, PICES Special
887 Publication 3, 2007.

888 Dowdeswell, J. A.: On the nature of Svalbard icebergs, *J Glaciol*, 35(120), 224-234, <https://org/10.3189/S002214300000455X>,
889 1989.

890 Egge, J. K., and Aksnes, D.L.: Silicate as regulating nutrient in phytoplankton competition, *Mar Ecol Prog ser.* Oldendorf, 83,
891 281-289, <https://org/10.3354/meps083281>, 1992.

892 Esau, I., and Repina, I.: Wind climate in Kongsfjorden, Svalbard, and attribution of leading wind driving mechanisms through
893 turbulence-resolving simulations, *Advances in Meteorology*, <https://org/10.1155/2012/568454>, 2012.

894 Fransson, A., Chierci, M., Nomura, D., Granskog, M. A., Kristiansen, S., Martma, T., and Nehrke, G.: Influence of glacialwater
895 and carbonate minerals on wintertime sea-ice biogeochemistry and the CO₂ system in an Arctic fjord in Svalbard, *Annals of*
896 *Glaciology*, 1–21, <https://doi.org/10.1017/aog.2020.52>, 2020.

897 Fransson, A., Chierici, M., Skjelvan, I., Olsen, A., Assmy, P., Peterson, A., Spreen, G., and Ward, B.: Effect of sea-ice and
898 biogeochemical processes and storms on under-ice water fCO₂ during the winter-spring transition in the high Arctic Ocean:
899 implications for sea-air CO₂ fluxes, *J. Geophys. Res. Oceans*, 122, 5566–5587, doi: 10.1002/2016JC012478, 2017.

900 Fofonoff, P., and Millard R. C.: Algorithms for computation of fundamental properties of seawater, *Unesco Technical Papers*
901 *in Marine Science*, 44, 53, <http://hdl.handle.net/11329/109>, 1983.

902 Fortier, M., Fortier, L., Michel, C., and Legendre, L.: Climatic and biological forcing of the vertical flux of biogenic particles
903 under seasonal Arctic sea ice, *Mar. Ecol. Prog. Ser.*, 225, 1-16, <https://org/10.3354/meps225001>, 2002.

904 Furnas, M. J.: In situ growth rates of marine phytoplankton: approaches to measurement, community and species growth rate,
905 J Plankton Res, 12, 1117–1151, 1990.

906 [Garrison, D. L., and Buck, K. R.: Organism losses during ice melting: a serious bias in sea ice community studies, Polar Biol](#)
 907 [6:237-239, 1986.](#)

908 Golden, K. M., Ackley, S. F., and Lytle, V. I.: The percolation phase transition in sea ice, *Science*, 282(5397), 2238-2241,
 909 <https://org/10.1126/science.282.5397.2238>, 1998.

910 Gradinger, R.: Sea ice microorganisms, *Encyclopedia of environmental microbiology*, Wiley,
 911 <https://org/10.1002/0471263397.env310>, 2003.

912 Gradinger, R.: Sea-ice algae: Major contributors to primary production and algal biomass in the Chukchi and Beaufort Seas
 913 during May/June 2002, *Deep Sea Res. Part II Top. Stud. Oceanogr.*, 56(17), 1201-1212,
 914 <https://org/10.1016/j.dsr2.2008.10.016>, 2009.

915 Granskog, M. A., Kaartokallio, H., and Shirasawa, K.: Nutrient status of Baltic Sea ice: Evidence for control by snow-ice
 916 formation, ice permeability, and ice algae, *J Geophys Res Oceans*, 108(C8), <https://org/10.1029/2002JC001386>, 2003.

917 Guardiola, M., Uriz, M. J., Taberlet, P., Coissac, E., Wangenstein, O. S., and Turon, X.: Deep-sea, deep-sequencing:
 918 metabarcoding extracellular DNA from sediments of marine canyons, *PloS one*, 10(10), e0139633, 2015.

919 Haecky, P., and Andersson, A.: Primary and bacterial production in sea ice in the northern Baltic Sea, *Aquat Microb Ecol*,
 920 20(2), 107-118, <https://org/10.3354/ame020107>, 1999.

921 Hagen, J. O., Liestøl, O., Roland, E., and Jørgensen, T.: *Glacier Atlas of Svalbard and Jan Mayen*, Oslo: Norwegian Polar
 922 Institute, 1993.

923 Halbach, L., Vihtakari, M., Duarte, P., Everett, A., Granskog, M. A., Hop, H., Kauko, H. M., Kristiansen, S., Myhre, P. I.,
 924 Pavlov, A. K., Pramanik, A., Tatarek, A., Torsvik, T., Wiktor, J. M., Wold, A., Wulff, A., Steen, H., Assmy, P.: Tidewater
 925 glaciers and bedrock characteristics control the phytoplankton growth environment in a fjord in the arctic, *Front Mar Sci*, 6,
 926 254, <https://org/10.3389/fmars.2019.00254>, 2019.

927 Hatton, J. E., Hendry, K. R., Hawkings, J. R., Wadham, J. L., Kohler, T. J., Stibal, M., Beaton, A. D., Bagshaw, E. A., and
 928 Telling, J.: Investigation of subglacial weathering under the Greenland Ice Sheet using silicon isotopes, *Geochim Cosmochim*
 929 *Acta*, 247, 191-206, <https://org/10.1016/j.gca.2018.12.033>, 2019.

930 Hawkings, J. R., Wadham, J. L., Benning, L. G., Hendry, K. R., Tranter, M., Tedstone, A., Nienow, P., and Raiswell, R.: Ice
 931 sheets as a missing source of silica to the polar oceans, *Nat. Commun*, 8(1), 1-10, <https://org/10.1038/ncomms14198>, 2017.

932 Hegseth, E. N., Assmy, P., Wiktor, J. M., Wiktor, J., Kristiansen, S., Leu, E., Tverberg, V., Gabrielsen, T. M., Skogseth, R.,
 933 and Cottier, F.: Phytoplankton seasonal dynamics in Kongsfjorden, Svalbard and the adjacent shelf, in: *The Ecosystem of*
 934 *Kongsfjorden, Svalbard*, edited by: Hop, H., and Wiencke, C., Springer, Cham., 173-227, 2019.

935 Hodal, H., Falk-Petersen, S., Hop, H., Kristiansen, S., and Reigstad, M.: Spring bloom dynamics in Kongsfjorden, Svalbard:
 936 nutrients, phytoplankton, protozoans and primary production, *Polar Biol* 35, 191–203, [https://doi.org/10.1007/s00300-011-](https://doi.org/10.1007/s00300-011-1053-7)
 937 [1053-7](https://doi.org/10.1007/s00300-011-1053-7), 2012.

938 Hodgkins, R.: Glacier hydrology in Svalbard, Norwegian high arctic, *Quat Sci Rev*, 16(9), 957-973, [https://org/10.1016/S0277-](https://org/10.1016/S0277-3791(97)00032-2)
 939 [3791\(97\)00032-2](https://org/10.1016/S0277-3791(97)00032-2), 1997.

940 Holmes, F. A., Kirchner, N., Kutteneuler, J., Krütfeldt, J., and Noormets, R.: Relating ocean temperatures to frontal ablation
 941 rates at Svalbard tidewater glaciers: Insights from glacier proximal datasets, *Sci. Rep.*, 9(1), 1-11, [https://org/10.1038/s41598-](https://org/10.1038/s41598-019-45077-3)
 942 019-45077-3, 2019.

943 Hopwood, M. J., Carroll, D., Dunse, T., Hodson, A., Holding, J. M., Iriarte, J. L., Ribeiro, S., Achterberg, E. P., Cantoni, C.,
 944 Carlson, D. F., Chierici, M., Clarke, J. S., Cozzi, S., Fransson, A., Juul-Pedersen, T., Winding, M. S. and Meire, L.: How does
 945 glacier discharge affect marine biogeochemistry and primary production in the Arctic?, *Cryosphere*, 14, 1347-1383, [https://org/](https://org/10.5194/tc-14-1347-2020)
 946 10.5194/tc-14-1347-2020, 2020.

947 Irvine-Fynn, T. D., Hodson, A. J., Moorman, B. J., Vatne, G., & Hubbard, A. L.: Polythermal glacier hydrology: A review,
 948 *Reviews of Geophysics*, 49(4), 2011.

949 Iversen, K. R., and Seuthe, L.: Seasonal microbial processes in a high-latitude fjord (Kongsfjorden, Svalbard): I. Heterotrophic
 950 bacteria, picoplankton and nanoflagellates, *Polar Biol.*, 34(5), 731-749, <https://org/10.1007/s00300-010-0929-2>, 2011.

951 Jones, E., Chierici, M., Skjelvan, I., Norli, M., Børsheim, K. Y., Lødemel, H. H., Sørensen, K., King, A. L., Lauvset, S.,
 952 Jackson, K., de Lange, T., Johannessen, T., and Mourgues, C.: Monitoring ocean acidification in Norwegian seas in 2018,
 953 Miljødirektoratet, M-1417/2019, 2019.

954 Kanna, N., Sugiyama, S., Ohashi, Y., Sakakibara, D., Fukamachi, Y., and Nomura, D.: Upwelling of macronutrients and
 955 dissolved inorganic carbon by a subglacial freshwater driven plume in Bowdoin Fjord, northwestern Greenland, *J Geophys*
 956 *Res Biogeosci.*, 123(5), 1666-1682, <https://org/10.1029/2017JG004248>, 2018.

957 Kartverket, <https://kartkatalog.geonorge.no/metadata/kartverket/dybdedata/2751aacf-5472-4850-a208-3532a51c529a>, last
 958 access: 10 August 2020.

959 Kirchman, D. L., Malmstrom, R. R., and Cottrell, M. T.: Control of bacterial growth by temperature and organic matter in the
 960 Western Arctic, *Deep Sea Research Part II: Topical Studies in Oceanography*, 52(24-26), 3386-3395, 2005.

961 Kowalik, Z., Marchenko, A., Brazhnikov, D., and Marchenko, N.: Tidal currents in the western Svalbard Fjords, *Oceanologia*,
 962 57(4), 318-327, <https://org/10.1016/j.oceano.2015.06.003>, 2015.

963 Krisch, S., Browning, T. J., Graeve, M., Ludwichowski, K.U., Lodeiro, P., Hopwood, M. J., Roig, S., Yong, J. C., Kanzow,
 964 T., and Achterberg, E. P.: The Influence of Arctic Fe and Atlantic Fixed N on Summertime Primary Production in Fram Strait,
 965 North Greenland Sea, Sci. Rep. 10 (1), 15230, <https://doi.org/10.1038/s41598-020-72100-9>, 2020.

966 Leppäranta, M., and Manninen, T.: The brine and gas content of sea ice with attention to low salinities and high temperatures,
 967 Finnish Institute of Marine Research Internal Report, 2, 1-15, 1988.

968 Láska, K., Witoszová, D., and Prošek, P.: Weather patterns of the coastal zone of Petuniabukta, central Spitsbergen in the
 969 period 2008–2010, *Polish Polar Research*, 297-318, 2012.

970 Leu, E., Mundy, C. J., Assmy, P., Campbell, K., Gabrielsen, T. M., Gosselin, M., Juul-Pedersen, T., and Gradinger, R.: Arctic
 971 spring awakening—Steering principles behind the phenology of vernal ice algal blooms, *Prog Oceanogr.*, 139, 151-170,
 972 <https://org/10.1016/j.pocean.2015.07.012>, 2015.

973 Lowry, K. E., Pickart, R. S., Selz, V., Mills, M. M., Pacini, A., Lewis, K. M., Joy-Warren, H., Nobre, C., van Dijken, G. L.,
 974 Grondin, P., Ferland, J., and Arrigo, K. R.: Under-ice phytoplankton blooms inhibited by spring convective mixing in
 975 refreezing leads, *J Geophys Res Oceans*, 123(1), 90-109, <https://org/10.1002/2016JC012575>, 2018.
 976 Lydersen, C., Assmy, P., Falk-Petersen, S., Kohler, J., Kovacs, K. M., Reigstad, M., Stehen, H., Strøm, H., Sundfjord, A.,
 977 Varpe, Ø., Walczowski, W., Weslawski, K. M., and Zajaczkowski, M.: The importance of tidewater glaciers for marine
 978 mammals and seabirds in Svalbard, Norway, *J Marine Sys*, 129, 452-471, <https://org/10.1016/j.jmarsys.2013.09.006>, 2014.
 979 Maes, S.: Polar cod population structure: connectivity in a changing ecosystem, Ph.D. thesis, KU Leuven, Leuven, Belgium,
 980 2017.
 981 Mahé, F., Rognes, T., Quince, C., de Vargas, C., and Dunthorn, M.: Swarm: robust and fast clustering method for amplicon-
 982 based studies, *PeerJ*, 2, e593, <https://org/10.7717/peerj.593>, 2014
 983 Massicotte, P., Bécu, G., Lambert-Girard, S., Leymarie, E., and Babin, M.: Estimating underwater light regime under spatially
 984 heterogeneous sea ice in the Arctic, *Appl. Sci.*, 8(12), 2693, <https://org/10.3390/app8122693>, 2018.
 985 Meire, L., Meire, P., Struyf, E., Krawczyk, D. W., Arendt, K. E., Yde, J. C., Juul Pedersen, T., Hopwood, M. J., Rysgaard, S.,
 986 and Meysman, F. J. R.: High export of dissolved silica from the Greenland Ice Sheet, *Geophys. Res. Lett.*, 43, 9173–9182,
 987 <https://doi.org/10.1002/2016GL070191>, 2016a.
 988 Meire, L., Mortensen, J., Rysgaard, S., Bendtsen, J., Boone, W., Meire, P., and Meysman, F. J.: Spring bloom dynamics in a
 989 subarctic fjord influenced by tidewater outlet glaciers (Godthåbsfjord, SW Greenland), *J Geophys Res Biogeosci*, 121(6),
 990 1581-1592, <https://org/10.1002/2015JG003240>, 2016b.
 991 Meslard, F., Bourrin, F., Many, G., and Kerhervé, P.: Suspended particle dynamics and fluxes in an Arctic fjord (Kongsfjorden,
 992 Svalbard), *Estuarine, Estuar Coast Shelf S*, 204, 212-224, <https://org/10.1016/j.ecss.2018.02.020>, 2018.
 993 Moskalik, M., Ćwiakała, J., Szczuciński, W., Dominiczak, A., Głowacki, O., Wojtysiak, K., and Zagórski, P: Spatiotemporal
 994 changes in the concentration and composition of suspended particulate matter in front of Hansbreen, a tidewater glacier in
 995 *Svalbard, Oceanologia*, 60(4), 446-463 2018.
 996 Mock, T., and Gradinger, R.: Determination of Arctic ice algal production with a new in situ incubation technique, *Mar. Ecol.*
 997 *Prog. Ser.*, 177, 15-26, <https://org/10.3354/meps177015>, 1999.
 998 Molari, M., Manini, E., and Dell'Anno, A.: Dark inorganic carbon fixation sustains the functioning of benthic deep-sea
 999 ecosystems, *Global Biogeochem Cycles*, 27(1), 212-221, <https://org/10.1002/gbc.20030>, 2013.
 1000 Moon, T., Sutherland, D. A., Carroll, D., Felikson, D., Kehrl, L., and Straneo, F.: Subsurface iceberg melt key to Greenland
 1001 fjord freshwater budget, *Nat Geosci*, 11(1), 49-54, <https://org/10.1038/s41561-017-0018-z>, 2018.
 1002 Mundy, C. J., Barber, D. G., and Michel, C.: Variability of snow and ice thermal, physical and optical properties pertinent to
 1003 sea ice algae biomass during spring, *J Marine Sys*, 58(3-4), 107-120, <https://org/10.1016/j.jmarsys.2005.07.003>, 2005.
 1004 Mundy, C. J., Gosselin, M., Ehn, J., Gratton, Y., Rossnagel, A., Barber, D. G., Martin, J., Tremblay, J., Palmer, M., Arrigo,
 1005 K. R., Darnis, G., Fortier, L., Else, B., Papakyriakou, T.: Contribution of under-ice primary production to an ice-edge upwelling
 1006 phytoplankton bloom in the Canadian Beaufort Sea, *Geophys. Res. Lett.*, 36(17), <https://org/10.1029/2009GL038837>, 2009.

1007 Natural Earth, <http://www.natureearthdata.com/>, last access: 10 August 2020.

1008 Norwegian Polar institute, Toposvalbard, <https://toposvalbard.npolar.no>, last access: 16 September 2020.

1009 Pabi, S., van Dijken, G. L., and Arrigo, K. R.: Primary production in the Arctic Ocean, 1998–2006, *J Geophys Res Oceans*,
 1010 113(C8), <https://org/10.1029/2007JC004578>, 2008.

1011 Parada, A. E., Needham, D. M., and Fuhrman, J. A.: Every base matters: assessing small subunit rRNA primers for marine
 1012 microbiomes with mock communities, time series and global field samples, *Environ. Microbiol.*, 18(5), 1403-1414,
 1013 <https://org/10.1111/1462-2920.13023>, 2016.

1014 Parsons, T. R., Maita, Y. and Lalli, C. M. (Eds.): *A Manual of Chemical and Biological Methods for Seawater Analysis*.
 1015 Pergamon Press, Toronto, 1984.

1016 Pavlov, A. K., Leu, E., Hanelt, D., Bartsch, I., Karsten, U., Hudson, S. R., Gallet, J., Cottier, F., Cohen, J. H., Berge, J.,
 1017 Johnsen, G., Maturilli, M., Kowalczyk, P., Sagan, S., Meler, J., and Granskog, M. A.: The underwater light climate in
 1018 Kongsfjorden and its ecological implications, in: *The Ecosystem of Kongsfjorden, Svalbard*, edited by: Hop, H., and Wiencke,
 1019 C., Springer, Cham., 137-170, 2019.

1020 Perovich, D. K., Roesler, C. S., and Pegau, W. S.: Variability in Arctic sea ice optical properties, *J Geophys Res Oceans*,
 1021 103(C1), 1193-1208, <https://org/10.1029/97JC01614>, 1998.

1022 Porter, K. G., and Feig, Y. S.: The use of DAPI for identifying and counting aquatic microflora1, *Limnol Oceanogr*, 25, 943–
 1023 948, <https://wiley.com/10.4319/lo.1980.25.5.0943>, 1980.

1024 Pruesse, E., Peplies, J., and Glöckner, F. O.: SINA: accurate high-throughput multiple sequence alignment of ribosomal RNA
 1025 genes, *Bioinformatics*, 28(14), 1823-1829, 2012.

1026 Ptacnik, R., Andersen, T., and Tamminen, T.: Performance of the Redfield ratio and a family of nutrient limitation indicators
 1027 as thresholds for phytoplankton N vs. P limitation, *Ecosystems*, 13(8), 1201-1214, <https://org/10.1007/s10021-010-9380-z>,
 1028 2010.

1029 Quast, C., Pruesse, E., Yilmaz, P., Gerken, J., Schweer, T., Yarza, P., Replies, J., and Glöckner, F. O.: The SILVA ribosomal
 1030 RNA gene database project: improved data processing and web-based tools. *Nucleic acids research*, 41(D1), D590-D596,
 1031 2012.

1032 Redfield, A. C.: On the proportions of organic derivatives in sea water and their relation to the composition of plankton, In
 1033 *James Johnstone Memorial Volume*, 176–192. Liverpool University Press, 1934.

1034 Rich, J., Gosselin, M., Sherr, E., Sherr, B., and Kirchman, D. L.: High bacterial production, uptake and concentrations of
 1035 dissolved organic matter in the Central Arctic Ocean, *Deep Sea Research Part II: Topical Studies in Oceanography*, 44(8),
 1036 1645-1663, 1997.

1037 Sager, J. C., and Mc Farlane, J. C.: Radiation, in: *Plant growth chamber handbook*, edited by: Langhans, R. W., and Tibbits,
 1038 T. W., Iowa Agr. Home Econ. Expt. Sta. Special Rpt, 99, 1-29, 1997.

1039 [Schaffer, J., and Kanzow, T.: von Appen, W. J.; von Albedyll, L.; Arndt, J. E.; Roberts, D. H. Bathymetry Constrains Ocean](#)
1040 [Heat Supply to Greenland's Largest Glacier Tongue, Nat. Geosci, 13\(3\), 227-231, \[https://doi.org/10.1038/s41561-019-0529-\]\(https://doi.org/10.1038/s41561-019-0529-x\)](#)
1041 [x, 2020.](#)

1042 Schoof, C., Rada, C. A., Wilson, N. J., Flowers, G. E., and Haseloff, M.: Oscillatory subglacial drainage in the absence of
1043 surface melt, *The Cryosphere*, 8(3), 959-976, 2014.

1044 Skogseth, R., Olivier, L. L., Nilsen, F., Falck, E., Fraser, N., Tverberg, V., Ledang, A. B., Vader, A., Jonassen, M. O., Søreide,
1045 J., Cottier, F., Berge, J., Ivanov, B. V., and Falk-Petersen, S.: Variability and decadal trends in the Isfjorden (Svalbard) ocean
1046 climate and circulation-an indicator for climate change in the European Arctic, *Prog Oceanogr*, 187, 102394,
1047 <https://org/10.1016/j.pocean.2020.102394>, 2020.

1048 Southwood, T. R. E. and Henderson, P. A. (Eds.): *Ecological methods*, John Wiley and Sons, 269, 2000.

1049 Strzelecki, M. C.: Schmidt hammer tests across a recently deglaciated rocky coastal zone in Spitsbergen-is there a "coastal
1050 amplification" of rock weathering in polar climates?, *Pol Polar Res*, 239-252, <https://org/10.2478/v10183-011-0017-5>, 2011.

1051 Sutherland, D. A., Pickart, R. S., Peter Jones, E., Azetsu-Scott, K., Jane Eert, A., and Ólafsson, J.: Freshwater composition of
1052 the waters off southeast Greenland and their link to the Arctic Ocean, *J Geophys Res Oceans*, 114(C5),
1053 <https://org/10.1029/2008JC004808>, 2009.

1054 [Sutherland, D. A., Straneo, F., & Pickart, R. S.: Characteristics and dynamics of two major Greenland glacial fjords, *Journal*](#)
1055 [of Geophysical Research: Oceans](#), 119(6), 3767-3791, 2014.

1056 Throndsen, J., Hasle, G. R., & Tangen, K. (Eds.): *Phytoplankton of Norwegian coastal waters*, Almatforlag AS, 2007.

1057 Tomas, C. R. (Ed.): *Identifying Marine Phytoplankton*, Elsevier, San Diego, 1997.

1058 Utermöhl, H.: Methods of collecting plankton for various purposes are discussed, *SIL Commun* 1953-1996. 9, 1-38,
1059 <https://doi.org/10.1080/05384680.1958.11904091>, 1958.

1060 [Van De Poll, W. H.; Kulk, G.; Rozema, P. D.; Brussaard, C. P. D.; Visser, R. J. W.; Buma, A. G. J. Contrasting Glacial](#)
1061 [Meltwater Effects on Post-Bloom Phytoplankton on Temporal and Spatial Scales in Kongsfjorden, Spitsbergen, *Elementa*,](#)
1062 [https://doi.org/10.1525/elementa.307, 2018.](#)

1063 Vihtakari, M.: PlotSvalbard: PlotSvalbard - Plot research data from Svalbard on maps. R package version 0.9.2,
1064 <https://github.com/MikkoVihtakari/PlotSvalbard>, 2020.

1065 von Quillfeldt, C. H.: Common diatom species in Arctic spring blooms: their distribution and abundance, *Bot Mar*, 43(6), 499-
1066 516, <https://org/10.1515/BOT.2000.050>, 2000.

1067 von Quillfeldt, C. H., Ambrose, W. G., and Clough, L. M.: High number of diatom species in first-year ice from the Chukchi
1068 Sea, *Polar Biol*, 26(12), 806-818, <https://org/10.1007/s00300-003-0549-1>, 2003.

1069 Vonnahme, T. R., Devetter, M., Žárský, J. D., Šabacká, M., and Elster, J.: Controls on microalgal community structures in
1070 cryoconite holes upon high Arctic glaciers, Svalbard, *Biogeosciences*, 13, 659-674, <https://org/10.5194/bg-13-659-2016>, 2016.

1071 Wadham, J. L., Hodgkins, R., Cooper, R. J., and Tranter, M.: Evidence for seasonal subglacial outburst events at a polythermal
1072 glacier, Finsterwalderbreen, Svalbard, *Hydrol. Process.*, 15(12), 2259-2280, <https://org/10.1002/hyp.178>, 2001.

1073 Wang, Q., Garrity, G. M., Tiedje, J. M., and Cole, J. R.: Naive Bayesian Classifier for Rapid Assignment of rRNA Sequences
1074 into the New Bacterial Taxonomy, *Appl Environ Microbiol.* 73(16), 5261-7, [https://org/ 10.1128/AEM.00062-07](https://org/10.1128/AEM.00062-07), 2007.

1075 Wangenstein, O. S., Palacín, C., Guardiola, M., and Turon, X.: DNA metabarcoding of littoral hard-bottom communities: high
1076 diversity and database gaps revealed by two molecular markers, *PeerJ*, 6, e4705, <https://org/10.7717/peerj.4705>, 2018.

1077 Wiedmann, I., Reigstad, M., Marquardt, M., Vader, A., and Gabrielsen, T. M.: Seasonality of vertical flux and sinking particle
1078 characteristics in an ice-free high arctic fjord—Different from subarctic fjords?, *J Marine Sys*, 154, 192-205,
1079 <https://org/10.1016/j.jmarsys.2015.10.003>, 2016.

1080 Wilson, N.: Characterization and interpretation of polythermal structure in two subarctic glaciers, Doctoral dissertation,
1081 Science: Department of Earth Sciences, 2012.

1082 Wynn, P. M., Hodson, A. J., Heaton, T. H., and Chenery, S. R.: Nitrate production beneath a High Arctic glacier, Svalbard,
1083 *Chemical geology*, 244(1-2), 88-102, 2007.

1084 yr.no, Longyearbyen – historikk, [https://www.yr.no/nb/historikk/graf/1-](https://www.yr.no/nb/historikk/graf/1-2759929/Norge/Svalbard/Svalbard/Longyearbyen?q=2019-04)
1085 [2759929/Norge/Svalbard/Svalbard/Longyearbyen?q=2019-04](https://www.yr.no/nb/historikk/graf/1-2759929/Norge/Svalbard/Svalbard/Longyearbyen?q=2019-04), last access: 24 July 2020.

1091 **Figures**

1092
1093

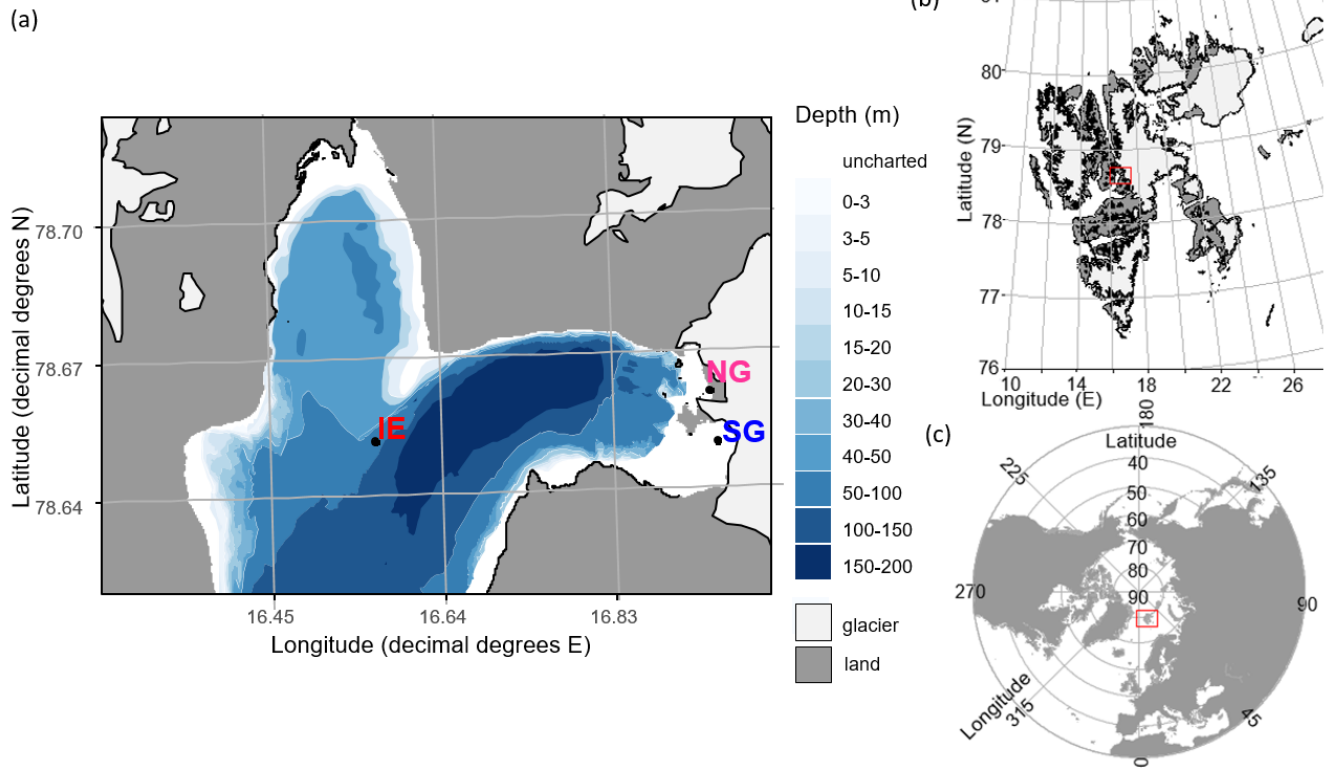


Fig 1. Sampling sites in Billefjorden: a) detailed Billefjorden map showing the stations at the ice edge (IE), north glacier (NG) and south glacier (SG) on the underlying bathymetric map. White areas are uncharted with water depths of about 30 m at NG and SG. The insets to the right show the location of b) Billefjorden on a Svalbard map and of c) Svalbard on a pan-Arctic map, marked with red boxes. Land is shown as dark grey, ocean as white, and glaciers as light grey. All maps were created using the PlotSvalbard R package (Vithakari, 2019). The Svalbard basemap is retrieved from the Norwegian Polar institute (2020, CC BY 4.0 license), the pan-Arctic map is retrieved from Natural Earth (2020, CC Public domain license), and the bathymetric map is retrieved from the Norwegian mapping authority (Kartverket, 2020, CC BY 4.0 license).

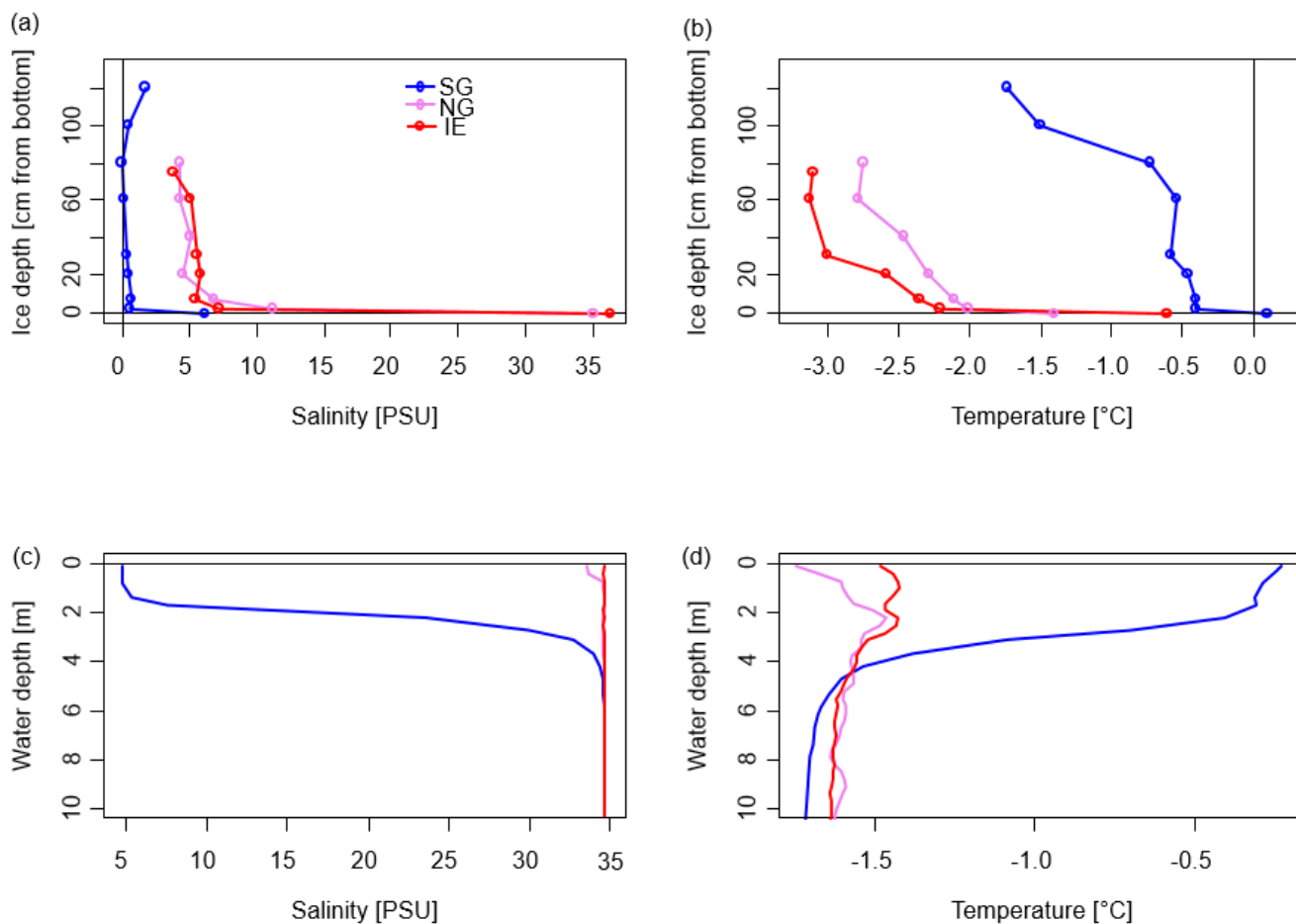


Fig 2. Bulk salinity and temperature profiles in a,b) sea ice cores (0 cm at the bottom) and c,d) the water column down to 10 m below the sea ice, of the three stations.

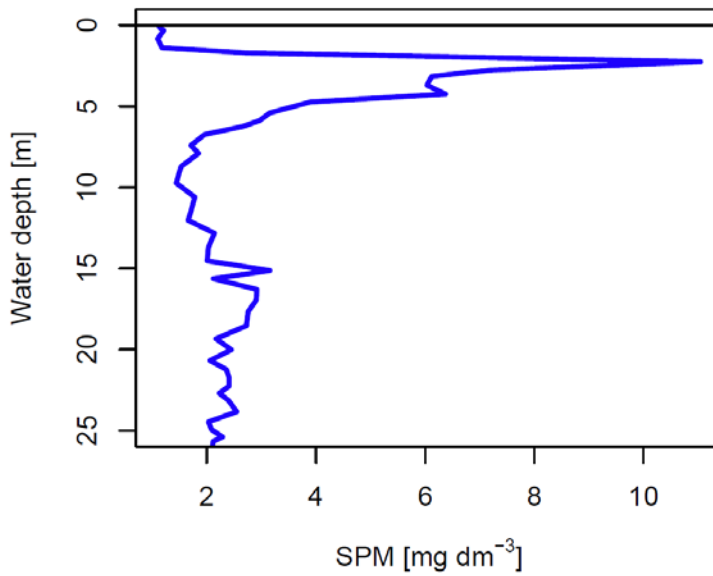
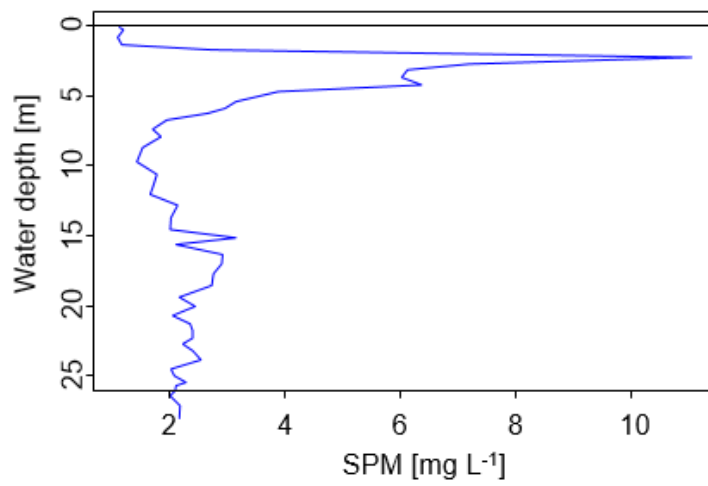


Fig 3. Turbidity profile of the SG station converted to suspended particles.

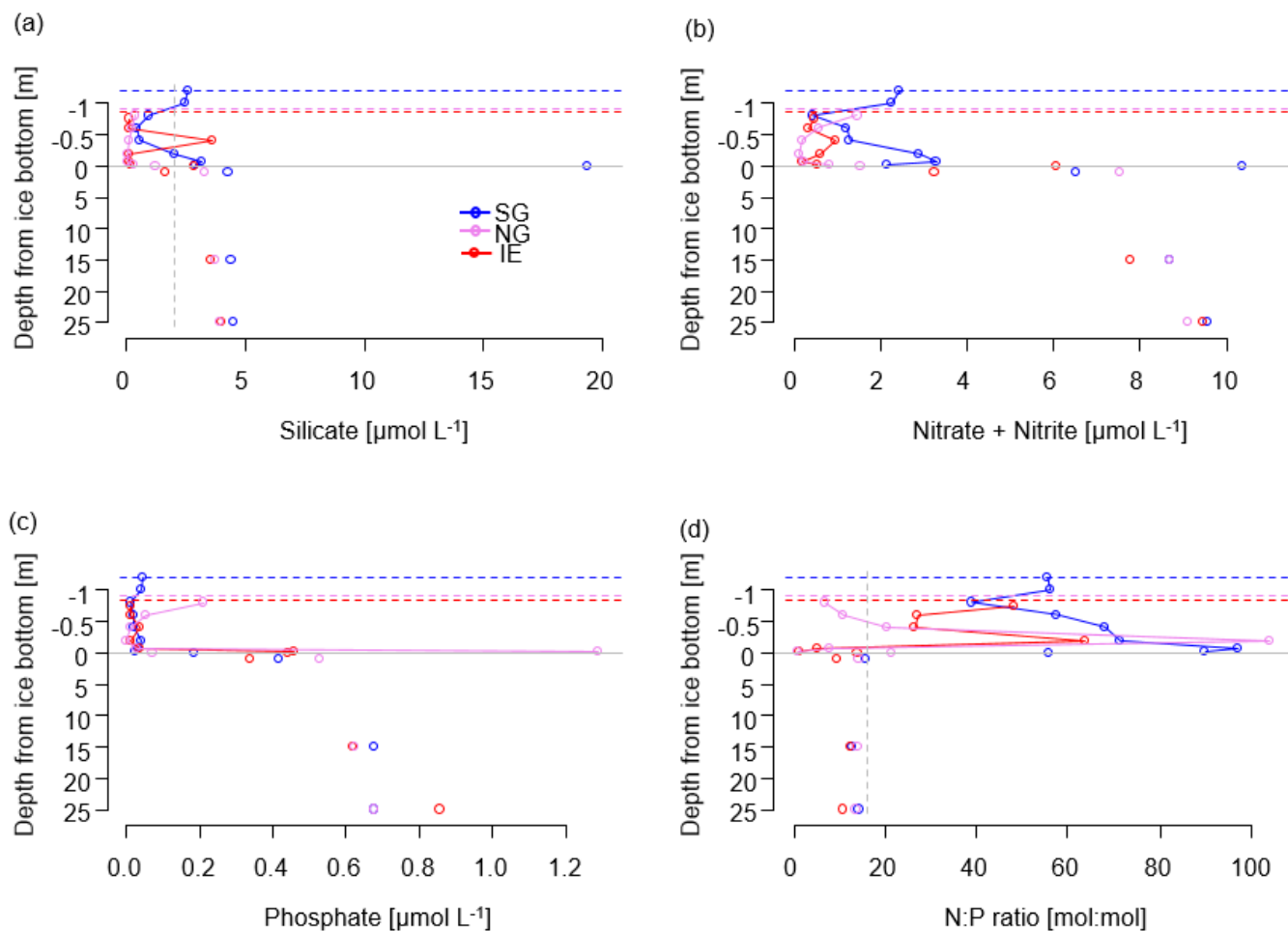
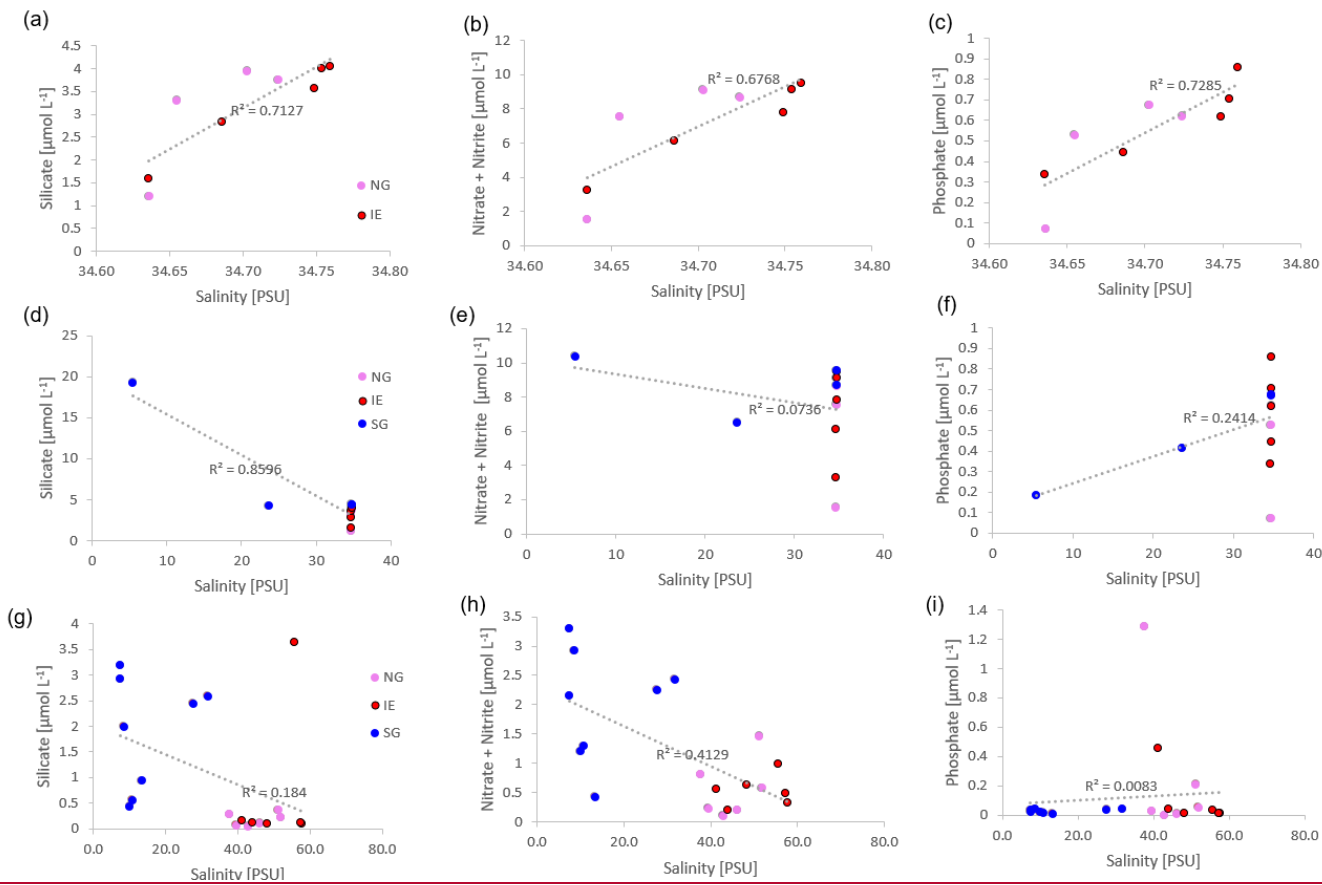


Fig 4. Nutrient concentrations in the water column (below grey line) and in sea ice (above the grey line) of a) silicate with a suggested threshold for limitation marked as dashed grey line, b) NO_x as nitrate and nitrite, c) phosphate and d) molar N:P ratios with the Redfield threshold of N:P 16:1 marked as dashed grey line indicating potential N limitation. Dashed lines indicate the position of the ice surface, while solid lines show the measured data.



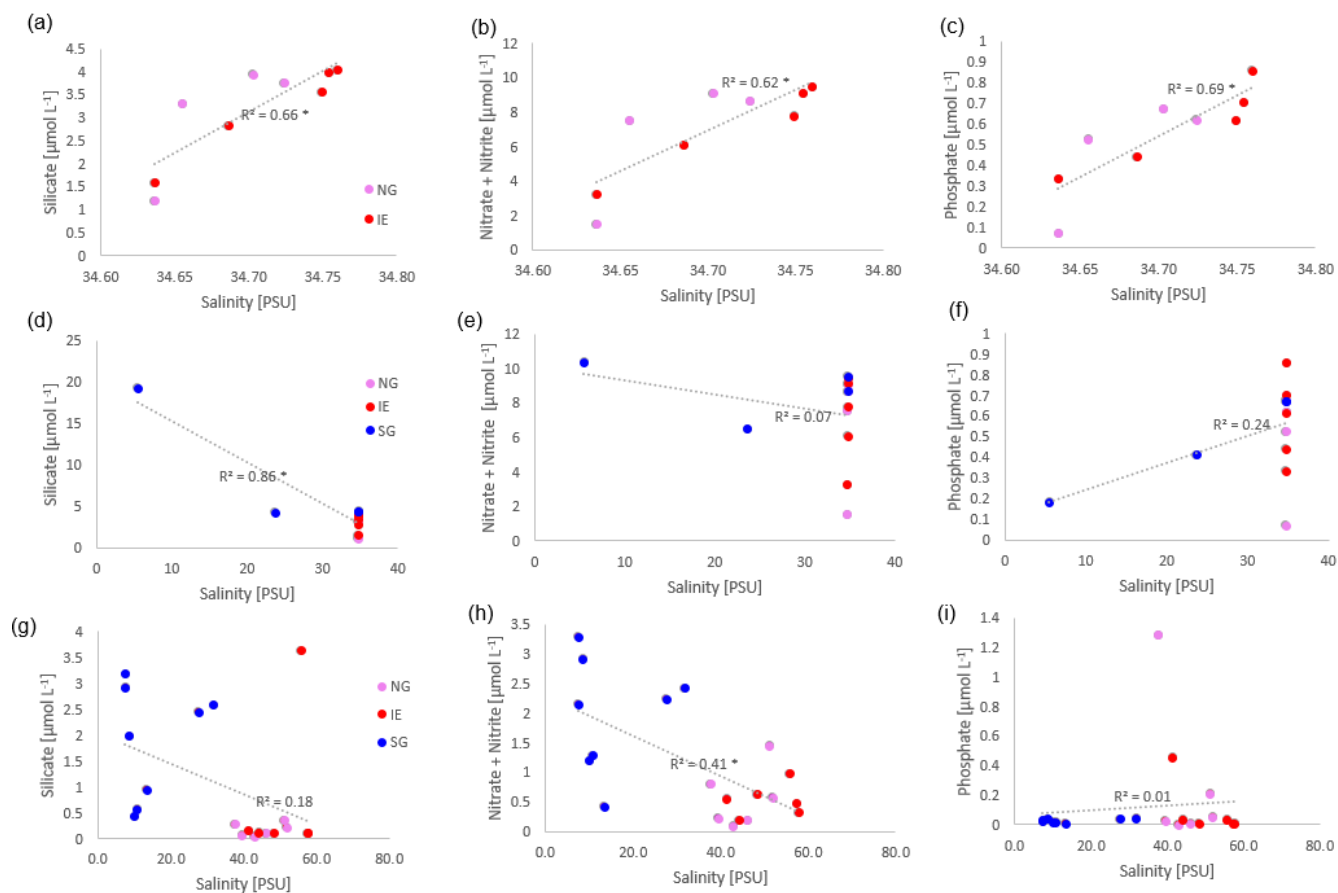
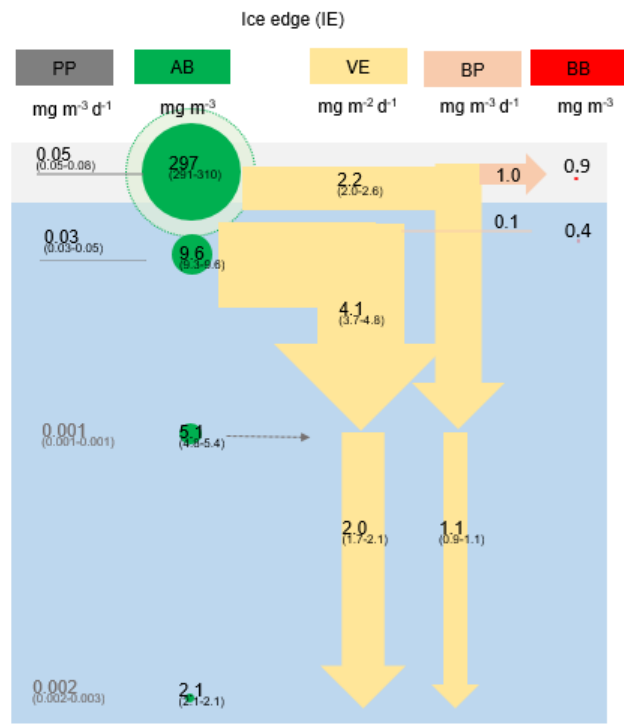
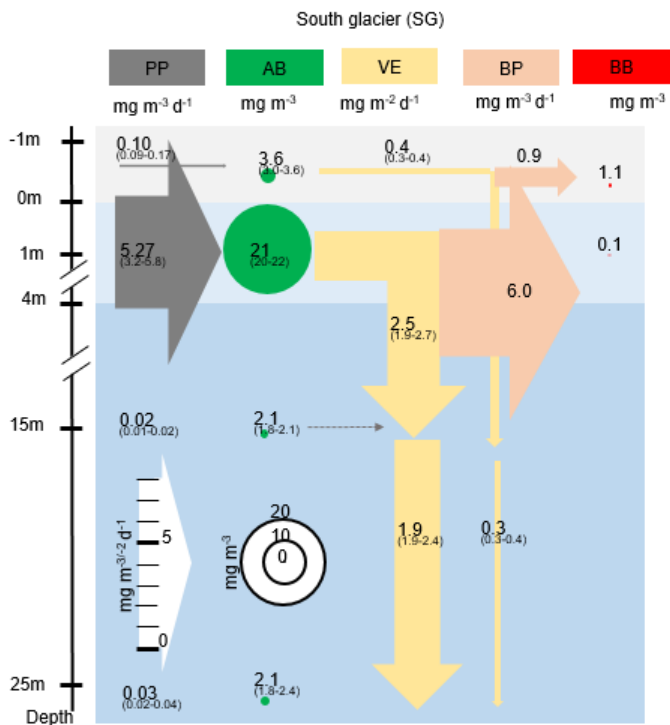


Fig 5. SalinityLinear salinity-nutrient correlations of NG and IE water samples (a-c), NG, IE, and SG water stations (d-f) and sea ice samples of NG, IE and SG (g-i). Conservative mixing showsA higher concentration in saline Atlantic water is shown as a positive correlation, non-conservative mixinga higher concentration in glacial meltwater as a negative correlation. Significant correlations ($p < 0.05$) are asterisk marked behind the R^2 value.



1134
1135
1136
1137
1138
1139
1140
1141
1142
1143
1144
1145
1146

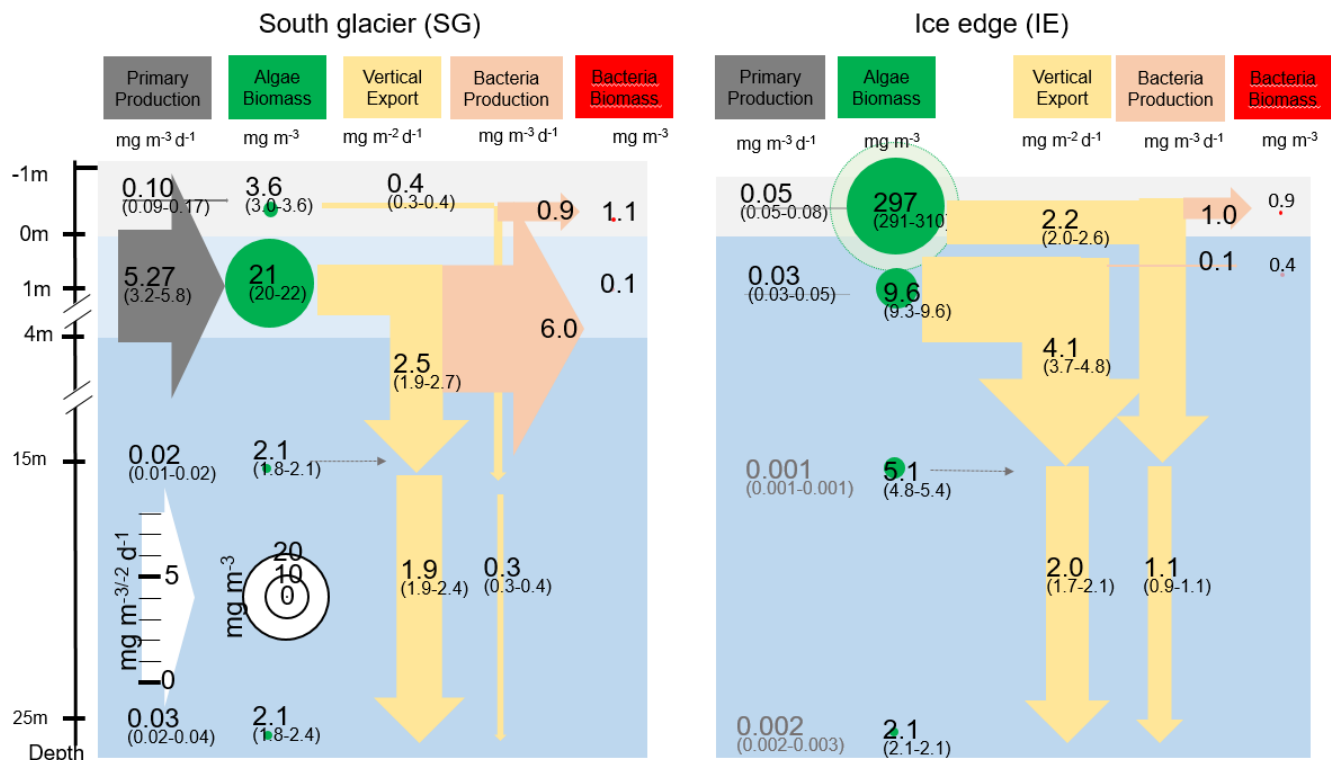
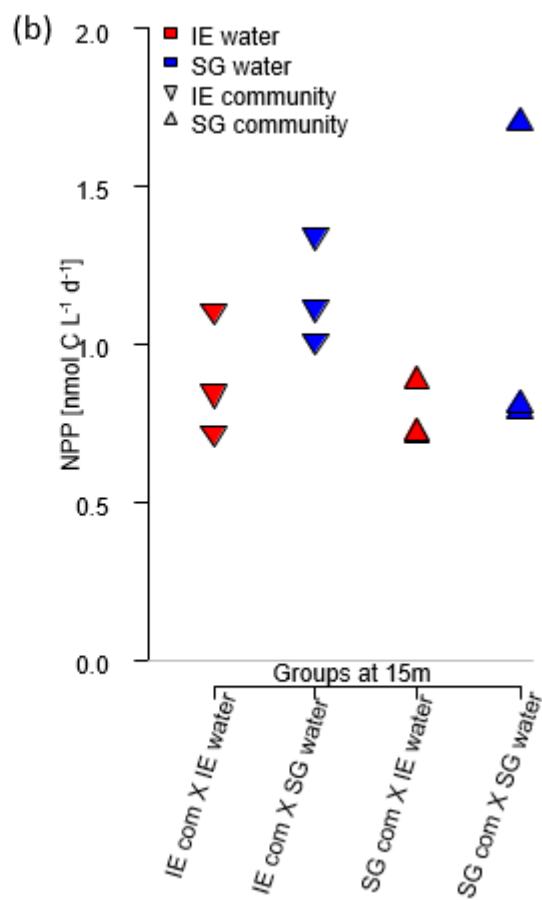
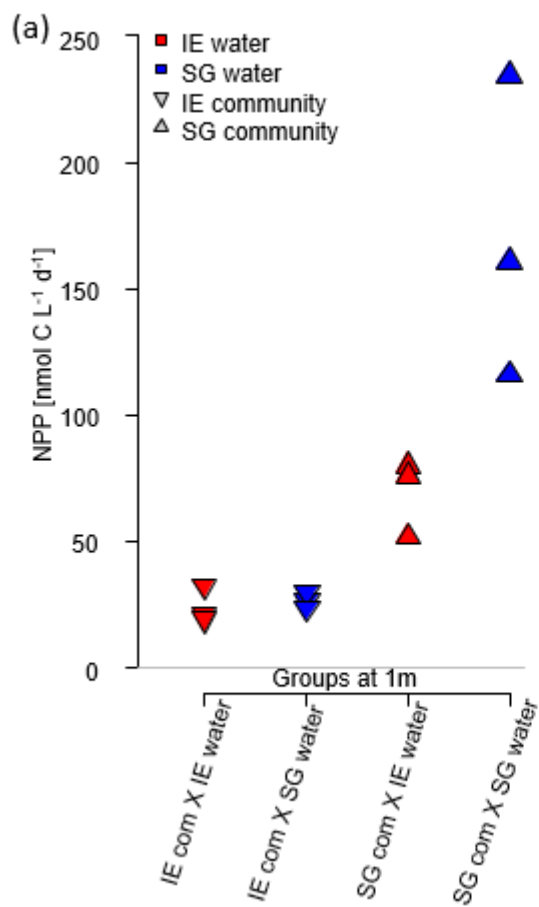


Fig 6. Schematic representation of the C cycle at SG and IE stations. All units are in mg C with the median given in the circles and arrows and the minimum and maximum in brackets below. 0 m depth is at the sea ice water interface. Grey arrows indicate net primary production (PP) with its height scaled to the uptake rates. Green circles show standing stock algae biomass (AB) converted from Chl to C (conversion factor = 30 gC gChl⁻¹, Cloern et al., 1995) with its diameter scaled to the concentrations, except sea ice at IE with the light green circle scaled one order of magnitude higher. Yellow arrows indicate vertical export (VE) of chlorophyll converted to C (conversion factor = 30 gC gChl⁻¹, Cloern et al., 1995) with the contribution of sea ice algae and phytoplankton estimated by the fraction of typical sea ice algae in phytoplankton net hauls and the width of the arrows scaled to the fluxes. Orange arrows indicate bacterial biomass production (BP) based on dark carbon fixation (conversion factor = 129 gC gDIC⁻¹, Molari et al., 2013) with the arrows scaled to the values. Red circles to the right are bacteria biomass (BB) assuming 20 fg C cell⁻¹ in the bottom sea ice and UIW. The grey area represents sea ice, the light blue area a brackish water layer and the darker blue area deeper saline water layers.



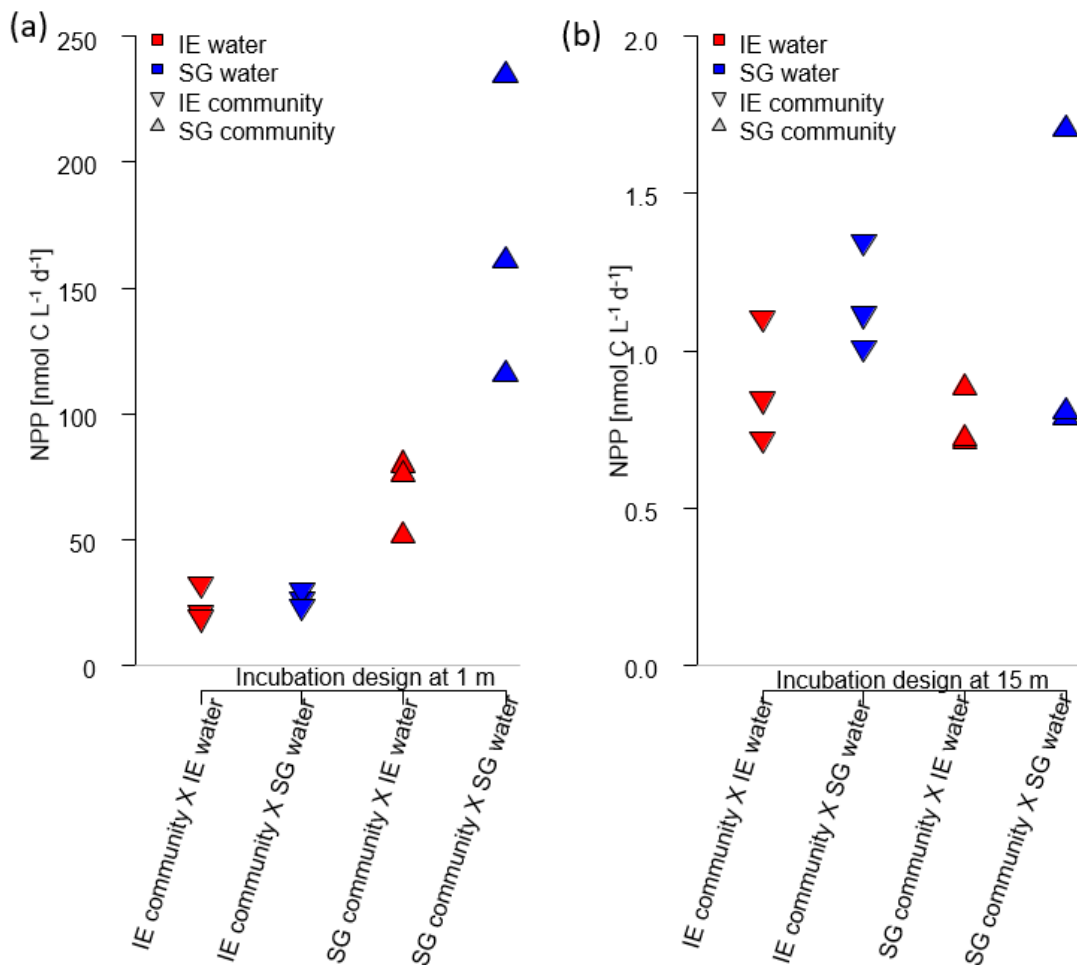
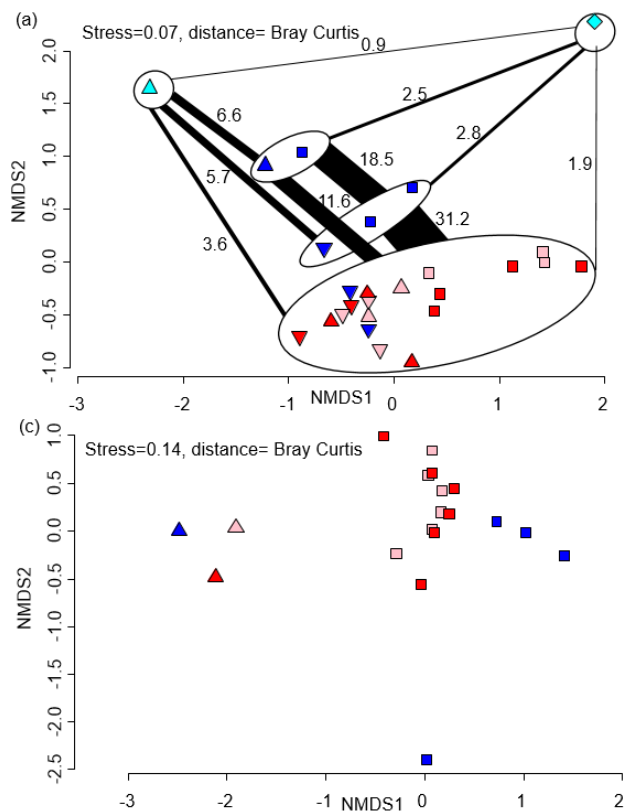


Fig 7. Impact of water source on primary production assessed via a reciprocal transplant experiment. Primary production of IE and SG communities incubated in sterile filtered water originated from either station at a) 1 m and b) 15 m depth. The symbols show the source of the community and the colors indicate the source of the sterile filtered incubation water. The type of incubation water (color) explains the variation in a nested ANOVA with community (symbol) and depth as nested constrained variables and water source (color) as explanatory variable ($p=0.0038$, $F=10.88$).



155

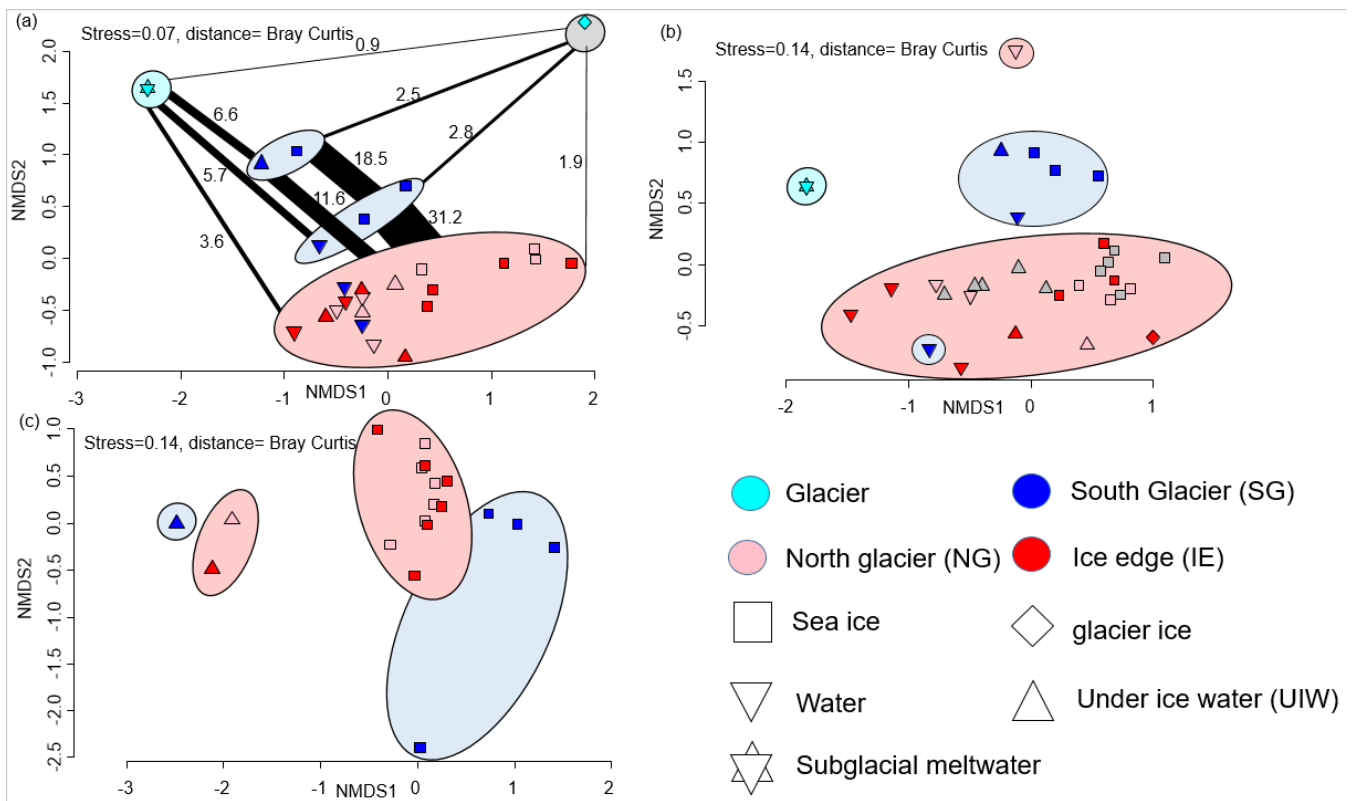


Fig 8. a) NMDS plot of microbial community structure based on 16S data (stress = 0.07), including samples from April 2018. Groups highlighted in eclipses: glacier ice (top right in grey eclipse), undiluted subglacial outflow (top left in cyan eclipse), surface samples (UIW, sea ice) at station SG 2019 (top blue eclipse), surface samples (1m water, sea ice) at station SG 2018 (bottom blue eclipse) and others including deeper water samples at SG (bottom in red eclipse). The fraction of shared OTUs (in %) are shown as lines scaled to the fraction [%] of shared OTUs. b) NMDS plot of community structure based on 18S data (stress = 0.14), including samples from April 2018 with the surface water sample of NG as outlier on top, and a surface water sample of SG as outlier in the pink reference cluster, c) NMDS plot based on algae abundances in sea ice and UIW based on light microscopic counts (stress = 0.14).

1173

1174 **Tables**

1175 Table 1. Properties of 1) marine surface and 2) Marine deep water (both station IE), 3) subglacial discharge melt water and 4)
1176 station SG surface water and the relative contribution of the water types 1 to 3 to form water type 4. The calculations are given
1177 in the Supplement and are based on different salinities and nutrients in the 4 water masses.~~the three identified water masses~~
1178 ~~and SG surface water and the estimated contributions of the different water masses based on salinity and different nutrients.~~

	<u>1) Surface water</u> <u>(IE 1 m)</u>		<u>2) Bottom water</u> <u>(IE)</u>		<u>3) Subglacial</u> <u>discharge</u> Meltwater		<u>4) SG</u> <u>(1 m)</u>
Salinity [PSU]	34.7		34.7		0 32 <u>± 0.1</u> %		23.6
Temperature [°C]	-1.4		-1.4		0		-0.4
Silicate [$\mu\text{mol L}^{-1}$]	1.59	0 %	4.46	<u>≥ 84</u> %	1.79	32 %	4.30
NO _x [$\mu\text{mol L}^{-1}$]	3.27	10 <u>± 3</u> %	9.57	58 <u>± 1</u> %	2.06	32 %	6.52
Phosphate [$\mu\text{mol L}^{-1}$]	0.34	19 <u>± 3</u> %	0.67	49 <u>± 3</u> %	0.09	32 %	0.42

1179

1180

1181

1182

1183

1184

1185

1186

1187

1188

1189

1190

1191

1192

1193

1194

1195

1196

1197

1198
1199
1200
1201
1202
1203
1204
1205
1206
1207
1208
1209
1210

Table 2. Integrated standing stock biomass of Chl and fluxes of Chl and C, fractions of the different fluxes and standing stocks, and bacterial production based on dark carbon fixation (DCF).

Variable	SG	IE	Unit
Chl int. in sea ice	0.02	0.40	mg m ⁻²
NPP in bottom sea ice	0.10	0.05	mg C m ⁻³ d ⁻¹
Chl int. in 25 m water column	3.74	3.75	mg m ⁻²
Vertical Chl flux to 25 m	0.07	0.11	mg Chl m ⁻² d ⁻¹
NPP at 1 m	5.27	0.03	mg C m ⁻³ d ⁻¹
C based NPP int. over 25 m	42.6	0.2	mg C m ⁻² d ⁻¹
Estimated Chl production int. over 25 m	1.4	0.0	mg C m ⁻² d ⁻¹
mg C fixed per mg Chl	11.4	0.1	mg C mg Chl d ⁻¹
NPP as fraction of Chl standing stock	38 %	0.2 %	% Chl renewal d ⁻¹
Doubling time	2.63	500	days
Vertical Chl flux as % of Chl standing stock	2 %	3 %	% export of Chl d ⁻¹
Vertical Chl flux as % of NPP based Chl prod.	5 %	1375 %	% export of NPP d ⁻¹
Loss of Chl from 15 to 25 m	12 %	19 %	Δexp 15m to 25m
Average Chl fraction of (Chl + Phaeo) in 0-3 cm ice	30%	85%	% Chl
Average Chl fraction of (Chl + Phaeo) in water	47 %	50 %	% Chl
Bacteria DCF ice	7.0	7.6	μg C m ⁻³ d ⁻¹
Bacteria Biomass prod (DCF based) ice	0.9	1.0	mg C m ⁻³ d ⁻¹
Doubling time	1.2	0.9	days
Bacteria DCF 1 m	46.9	1.1	μg DIC m ⁻³ d ⁻¹
Bacteria Biomass prod (DCF based) 1m	6.0	0.1	mg C m ⁻³ d ⁻¹
Doubling time	0.02	2.9	days

1211 Appendix

1212 Equations 1-6. Mixing calculations for estimates of the fraction of meltwater (MW_{Sal}) based on salinity, and for bottom water
 1213 based on nutrient concentrations (BW_{Nuts}). Sal indicates the average salinities measured at the IE (Sal_{IE}), SG at 1m depth
 1214 (Sal_{SG1m}), subglacial outflow (Sal_{glac}). Nut indicates the nutrient concentrations of nitrate and nitrite (NO_x), silicate (Si), and
 1215 phosphate (PO_4) at 1m under the sea ice at SG (Nut_{1mSG}) and IE (Nut_{1mIE}), the bottom water of the IE (Nut_{BW}), or subglacial
 1216 outflow water (Nut_{glac}).

$$1218 \quad MW_{Sal}[\%] = \frac{Sal_{IE} - Sal_{SG1m}}{Sal_{SG1m} - Sal_{glac} + Sal_{IE} - Sal_{SG1m}} * 100 \quad (1)$$

$$1219 \quad MW_{Sal}[\%] = \frac{34.7 \text{ PSU} - 23.6 \text{ PSU}}{23.6 \text{ PSU} - 0 \text{ PSU} + 34.7 \text{ PSU} - 23.6 \text{ PSU}} * 100 = 32 \% \quad (2)$$

$$1221 \quad BW_{Nut}[\%] = \frac{Nut_{1mSG} - MW_{Sal}[\%] * Nut_{glac} - Nut_{1mIE} + MW_{Sal}[\%] * Nut_{1mIE}}{Nut_{BW} - Nut_{1mIE}} * 100 \quad (3)$$

$$1223 \quad BW_{NOx}[\%] = \frac{6.52 \mu M - 0.32 * 2.06 \mu M - 3.27 \mu M + 0.32 * 3.27 \mu M}{9.57 \mu M - 3.27 \mu M} * 100 = 58 \% \quad (4)$$

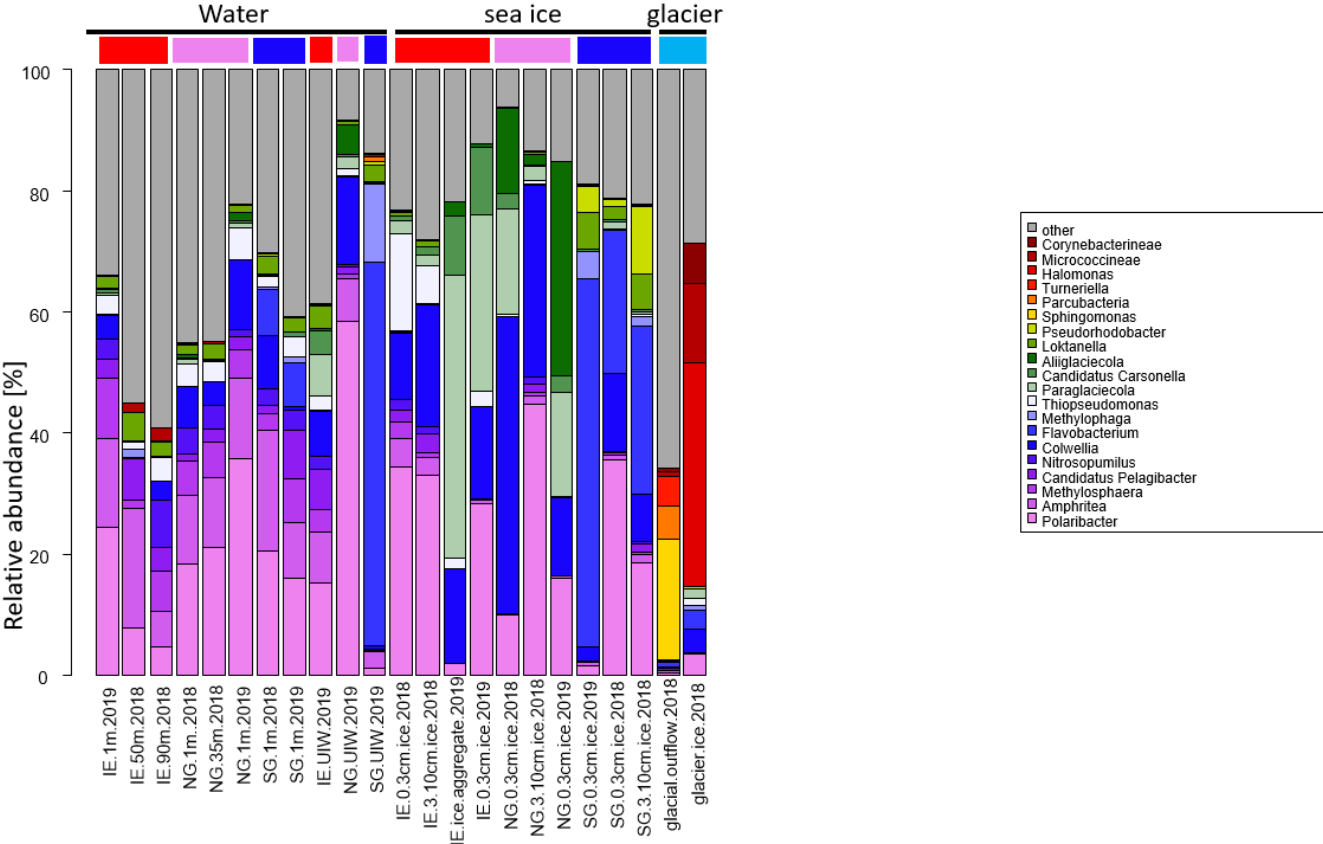
$$1225 \quad BW_{Si}[\%] = \frac{4.30 \mu M - 0.32 * 1.79 \mu M - 1.59 \mu M + 0.32 * 1.59 \mu M}{4.46 \mu M - 1.59 \mu M} * 100 = 92 \% \quad (5)$$

$$1227 \quad BW_{PO4}[\%] = \frac{0.41 \mu M - 0.32 * 0.09 \mu M - 0.34 \mu M + 0.32 * 0.34 \mu M}{0.67 \mu M - 0.34 \mu M} * 100 = 46 \% \quad (6)$$

1229 Equation 7. Calculation of vertical flux of Chl based on the sediment traps with concentration of Chl (C), Volume in the
 1230 sediment trap cylinder (V), area above the cylinder (A) and incubation time (t).

$$1231 \quad \text{Vertical flux} = \frac{C * V}{A * t} \quad (7)$$

1245
1246
1247
1248



1249
1250
1251
1252
1253
1254
1255
1256
1257
1258
1259
1260

Fig. A1. Community composition of the most abundant genera based on 16S rRNA sequencing data.

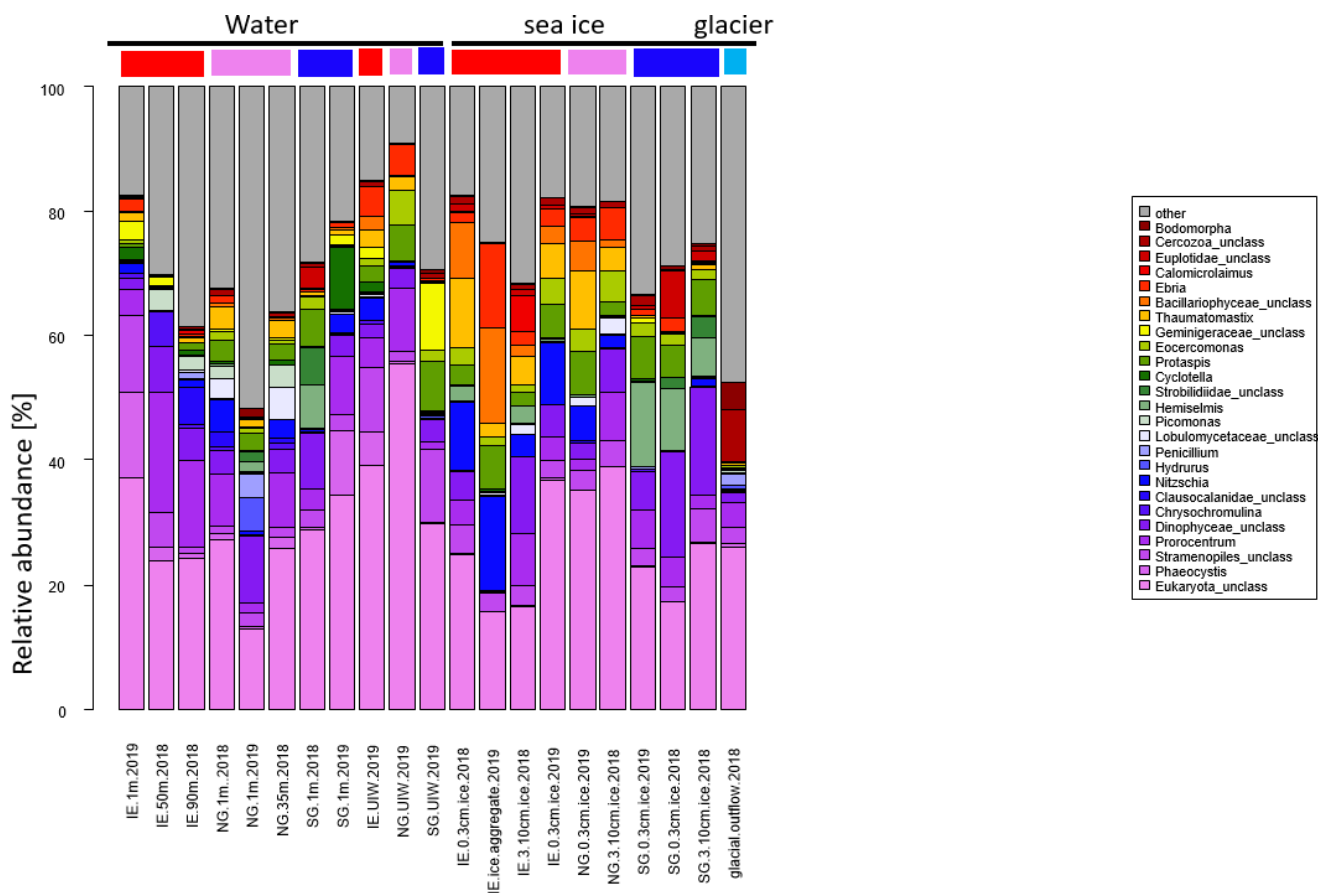
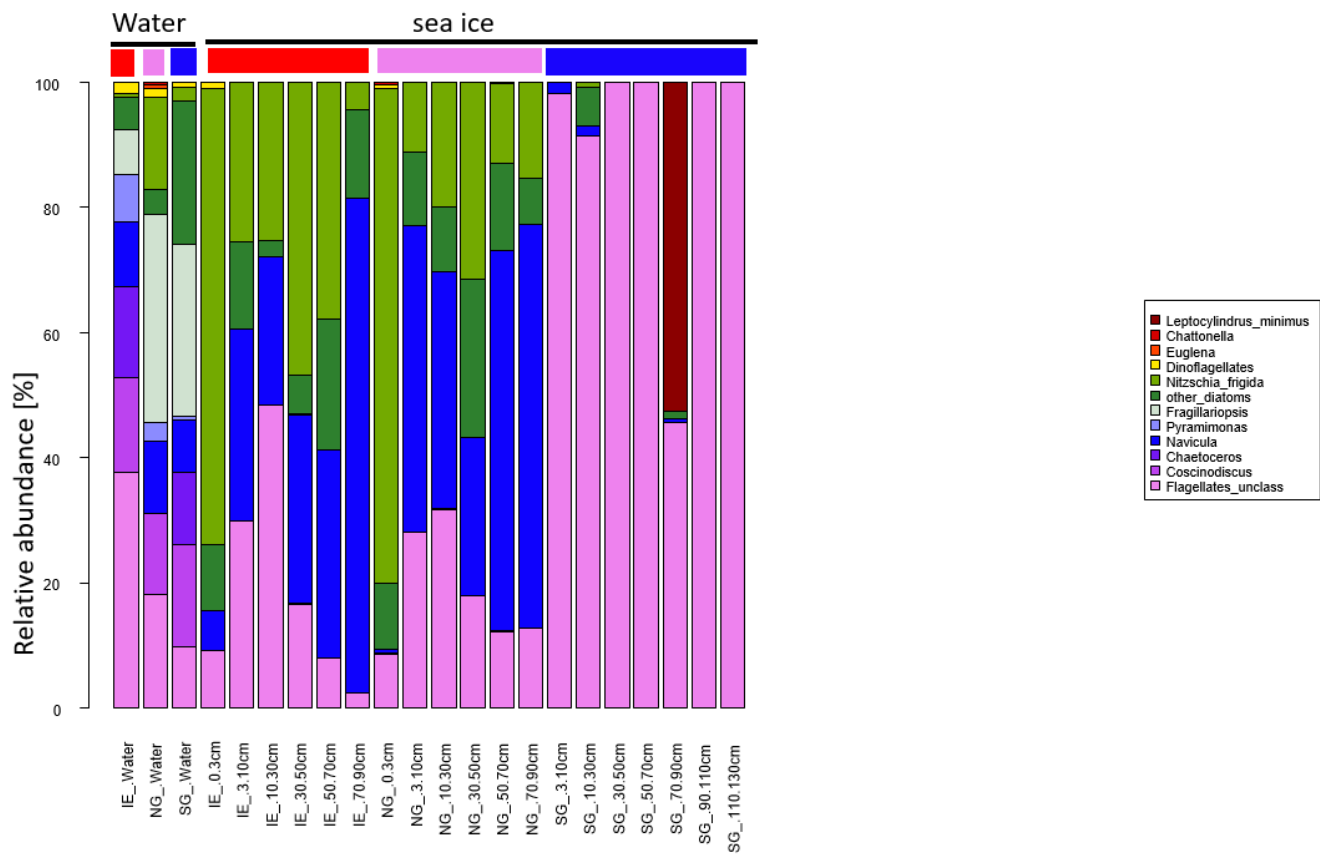


Fig. A2. Community composition based on 18S rRNA sequencing data of the most abundant genera or highest taxonomic level if no related genus has been found.

1276
1277
1278
1279
1280



1281
1282
1283
1284
1285
1286
1287
1288
1289
1290

Fig. A3. Sea ice algae and UIW algae community composition of the most abundant taxonomic groups based on light microscopy.

~~Table B1. Sea ice properties and conversions from bulk salinity and temperature to brine salinity, densities, and brine volume fractions.~~

	Ice—core section [cm]	Temp [°C]	Brine Sal [PSU]	Ice density [kg·m ⁻³]	Brine density [kg·m ⁻³]	Brine—volume fraction
SG	0 to 3	-0.4	7.4	917.1	1005.9	7 %
	3 to 10	-0.4	7.4	917.1	1005.9	9 %
	10 to 30	-0.5	8.5	917.1	1006.8	5 %
	30 to 50	-0.6	10.7	917.1	1008.6	3 %
	50 to 70	-0.5	10.0	917.1	1008.0	1 %
	70 to 90	-0.7	13.3	917.1	1010.6	0 %
	90 to 100	-1.5	27.6	917.2	1022.0	1 %
-	110 to 130	-1.7	31.7	917.2	1025.4	5 %
NG	0 to 3	-2.0	37.6	917.3	1030.0	28 %
	3 to 10	-2.1	39.4	917.3	1031.6	16 %
	10 to 30	-2.3	42.8	917.3	1034.2	10 %
	30 to 50	-2.5	46.1	917.3	1036.9	10 %
	50 to 70	-2.8	51.8	917.4	1041.4	8 %
-	70 to 92	-2.7	51.1	917.4	1040.9	8 %
IE	0 to 3	-2.2	41.3	917.3	1033.1	16 %
	3 to 10	-2.4	44.1	917.3	1035.3	11 %
	10 to 30	-2.6	48.3	917.4	1038.6	11 %
	30 to 50	-3.0	55.6	917.4	1044.5	9 %
	50 to 70	-3.1	57.7	917.4	1046.2	8 %
-	70 to 80	-3.1	57.3	917.4	1045.9	6 %

1304
1305
1306
1307
1308

Table B2. Geographic metadata and nutrient concentrations in $\mu\text{mol L}^{-1}$ related to Billefjorden.

					Depth	Si(OH)_4	NO_x	PO_4	N:P
Depth	Station	Latitude (N)	Longitude (E)	type	[m]	$[\mu\text{mol L}^{-1}]$	$[\mu\text{mol L}^{-1}]$	$[\mu\text{mol L}^{-1}]$	$[\text{mol mol}^{-1}]$
UIW	SG	78°39'03	16°56'44	water	0.01	19.3	10.4	0.19	55.8
1-m	SG	78°39'03	16°56'44	water	1	4.3	6.5	0.42	15.7
15-m	SG	78°39'03	16°56'44	water	15	4.4	8.7	0.68	12.9
25-m	SG	78°39'03	16°56'44	water	25	4.5	9.6	0.67	14.2
UIW	NG	78°39'40	16°56'19	water	0.01	1.2	1.5	0.07	21.4
1-m	NG	78°39'40	16°56'19	water	1	3.3	7.6	0.53	14.3
15-m	NG	78°39'40	16°56'19	water	15	3.8	8.7	0.62	14.0
25-m	NG	78°39'40	16°56'19	water	25	4.0	9.1	0.68	13.5
UIW	IE	78°39'09	16°34'01	water	0.01	2.8	6.1	0.44	13.8
1-m	IE	78°39'09	16°34'01	water	1	1.6	3.3	0.34	9.7
15-m	IE	78°39'09	16°34'01	water	15	3.6	7.8	0.62	12.6
25-m	IE	78°39'09	16°34'01	water	25	4.0	9.5	0.86	11.1
Bot	IE	78°39'09	16°34'01	water	57	4.0	9.1	0.70	13.0
0-3-cm	IE	78°39'09	16°34'01	Sea-ice	-1.5	0.2	0.6	0.46	1.2
3-10-cm	IE	78°39'09	16°34'01	Sea-ice	-6.50	0.1	0.2	0.04	5.1
10-30-cm	IE	78°39'09	16°34'01	Sea-ice	-20	0.1	0.6	0.01	63.5
30-50-cm	IE	78°39'09	16°34'01	Sea-ice	-40	3.6	1.0	0.04	26.6
50-70-cm	IE	78°39'09	16°34'01	Sea-ice	-60	0.1	0.3	0.01	27.1
70-80-cm	IE	78°39'09	16°34'01	Sea-ice	-75	0.1	0.5	0.01	48.1
0-3-cm	NG	78°39'40	16°56'19	Sea-ice	-1.5	0.3	0.8	1.29	0.6
3-10-cm	NG	78°39'40	16°56'19	Sea-ice	-6.50	0.1	0.2	0.03	7.9
10-30-cm	NG	78°39'40	16°56'19	Sea-ice	-20	0.0	0.1	0.00	104.0
30-50-cm	NG	78°39'40	16°56'19	Sea-ice	-40	0.1	0.2	0.01	20.3
50-70-cm	NG	78°39'40	16°56'19	Sea-ice	-60	0.2	0.6	0.05	10.9
70-90-cm	NG	78°39'40	16°56'19	Sea-ice	-80	0.4	1.5	0.21	6.9
0-3-cm	SG	78°39'03	16°56'44	Sea-ice	-1.5	2.9	2.2	0.02	89.8
3-10-cm	SG	78°39'03	16°56'44	Sea-ice	-6.50	3.2	3.3	0.03	97.1
10-30-cm	SG	78°39'03	16°56'44	Sea-ice	-20	2.0	2.9	0.04	71.2

30-50 cm	SG	78°39'03	16°56'44	Sea ice	-40	0.6	1.3	0.02	68.1
50-70 cm	SG	78°39'03	16°56'44	Sea ice	-60	0.4	1.2	0.02	57.6
70-90 cm	SG	78°39'03	16°56'44	Sea ice	-80	0.9	0.4	0.01	38.9
90-110 cm	SG	78°39'03	16°56'44	Sea ice	-100	2.4	2.3	0.04	56.3
110-130 cm	SG	78°39'03	16°56'44	Sea ice	-120	2.6	2.4	0.04	55.4

1309

1310

1311

1312 Table B3. Geographic metadata and nutrient concentrations related to Nordenskiöldbreen.

Date	Stat	Lat (N)	Lon (E)	type	Silicate [μmol L ⁻¹]	NO _x [μmol L ⁻¹]	Phosphate [μmol L ⁻¹]	Nitrite [μmol L ⁻¹]	Nitrate [μmol L ⁻¹]
09.07.2018	NC	78°38'3	16°59'4	Cryoconite	0.18	0.741	0.597	0.133	0.608
09.07.2018	NC	78°38'3	16°59'4	Cryoconite	0.179	0.555	0.75	0.084	0.471
09.07.2018	NC	78°38'3	16°59'4	Cryoconite	0.066	0.732	0.332	0.069	0.663
09.07.2018	NC	78°38'3	16°59'4	Cryoconite	0.157	0.674	1.281	0.067	0.607
09.07.2018	NC	78°38'3	16°59'4	Cryoconite	0.044	0.681	0.163	0.052	0.629
09.07.2018	NR	78°39'3	16°56'5	Cryoconite	0.323	0.537	0.611	0.311	0.226
09.07.2018	NR	78°39'3	16°56'5	Cryoconite	0.073	0.671	0.201	0.07	0.601
09.07.2018	NR	78°39'3	16°56'5	Cryoconite	0.062	0.361	0.383	0.077	0.284
09.07.2018	NR	78°39'3	16°56'5	Cryoconite	0.146	0.609	0.222	0.113	0.496
09.07.2018	NR	78°39'3	16°56'5	Cryoconite	0.049	0.53	0.26	0.065	0.465
25.04.2018	Out	78°38'2	16°75'2	outflow	1.535	2.304	0.083	0.009	2.295
25.04.2018	Out	78°38'2	16°75'2	outflow	2.047	1.814	0.096	0.013	1.801
25.04.2018	NC	78°38'3	16°59'4	glacier ice	0.085	0.928	0.038	0.008	0.92

1313

1314

1315

1316

1317

1318

1319

1320

1321

1322

1323

1324
1325
1326